The Origin of Endorheic Pans on The African Erosion Surface North of Grahamstown, South Africa

MSc Thesis

JUDITH ALISTOUN

Judith Alistoun

Environmental Science

Abstract

Pans on the African Erosion Surface near Grahamstown are small features, which, perhaps due to their small size have been neglected by researchers. From the outset the striking difference of these pans relative to other pans in southern Africa, is that the host rock is silcrete, a highly resistant rock well known as being associated with deeply weathered plateaus. The dominant origin theory for pans in southern Africa was developed by Goudie and Thomas (1985), and focuses on mechanisms relating to erosion and deflation. This model does not fit in well with the pans that have formed on substrate that has largely been unaffected by erosion in recent geological history (thousands to 10 000 years). As such this study examined the role of prolonged chemical weathering of Dwyka Tillite, that has led to the formation of silcrete. The hypothesis was that such deep weathering is responsible for local scale volume changes, which have in turn led to the formation of a depression.

The centre of the pan indicated the highest concentration of Al_2O_3 and kaolinite at mid depths, and their concentrations decreased vertically away from these depths, and laterally towards the margins of the pan. Similar results were noted for SiO_2, while CaO and MgO (and calcite and dolomite) were highest at mid depths along the margins of the pan, and decreased laterally toward the centre of the pan. Results indicated that there was a positive relationship in the centre of the pan between:

- *the degree of chemical weathering and volume losses,*
- *relative elevation of the pan and volume changes.*

Geochemically and mineralogically, there was a link between the high concentrations of Ca and Mg carbonates and volume gains in the margin of the pans. It is proposed that transpiration of vegetation along the margin of the pan caused the lateral movement of solutes, and the selective exclusion of these solutes by plants was associated with carbonate precipitation, leading to the creation of local relief. These results provide evidence to suggest that weathering and precipitation processes occurring over geological time scales are responsible for minor scale relief features, whose origin has been mistakenly attributed to deflation processes occurring over hundreds to thousands of years.

Acknowledgements

I would like to extent my sincere gratitude to the following people whose contributions have made this thesis possible:

1. Prof Fred Ellery, my supervisor, for your unending patience, direction, insights and encouragement. You have been an incredibly supportive and kind supervisor. Your tendency to always be constructive in your guidance has helped me enormously during this process. I feel incredibly grateful for all you have done for me.
2. Garth, my husband, your love and support have been my crutch, and words are simply inadequate to relay how much I have appreciated your presence over the last few years.
3. To my family for your care, love and support through my endeavour.
4. To my friends for keeping the smile on my face, and being available to provide emotional and spiritual support whenever needed.
5. To the NRF who funded my research.

Table of Contents

List of Figures

List of Tables

List of Equations

Chapter 1: Introduction

1.1 Background

Wetland Science in South Africa has been dominated by ecologists; with only very recent input from hydrologists, soil scientists and geomorphologists to the field (McCarthy and Hancox, 2000). Without understanding the geomorphological and geological controls on wetland formation, and the processes that operate to influence wetland dynamics, wetland management is likely to be relatively unsuccessful in South Africa. Ellery *et al*. (2009) and McCarthy and Hancox (2000) argue that it is crucial to have an understanding of the processes which are responsible for wetland occurrence and dynamics so that management and rehabilitation "work with rather than against nature".

Endorheic pans are round or kidney shaped features which are located in closed basins or in topographic depressions (Shaw and Thomas, 1997). Seasonal interaction with surface water and groundwater, particularly the predominance of evaporation as the dominant component of the water balance, are responsible for the well-known occurrence of salt pans (Allan *et al*., 1995), which is perhaps how pans are best known. Many pans have become popular tourist attractions such as Etosha and Makgadikgadi Pans in Namibia and Botswana respectively.

Endorheic pans are the most common type of wetland in arid to semi-arid climatic regions (Allan *et al.*, 1995). In southern Africa pans typically occur in regions with less than 500 mm mean annual rainfall (Goudie and Wells, 1995) and even occur widely in the southern Kalahari, which receives less than 200 mm of rain annually (Thomas and Shaw, 1991). The predominant model to describe pan formation was developed by Goudie and Thomas (1985) on the basis of environmental processes that are widely associated with arid and semi-arid environments, and act in conjunction with one another to form pans. Such factors include low precipitation, limited vegetation, and the presence of flat to gently sloping topography in combination with heavy grazing, wind erosion and deflation.

Pans are however also widespread in areas that receive greater than 500 mm rainfall per annum; most notably the Highveld of Mpumalanga Province in South Africa, which hosts numerous pans including the globally significant "Lake Chrissie" – a pan of considerable extent at over 6 km in length and 2 km in width (Allan *et al*., 2005). Rainfall in this region is approximately 800 mm per annum. Distribution of pans over a wide range of climatic conditions, particularly with respect to mean annual rainfall, presents difficulty in explaining pan formation based on arid to semi-arid processes and features, such as deflation and sparse vegetation. An alternative model is therefore required to explain pan origin in moist areas where loss of vegetation due to animal activity is not likely to be sufficiently high for pan formation. The case of Nyamvubu Vlei in Kwazulu-Natal, South Africa, where long term weathering of dolerite on the African Erosion Surface has led to subsidence of the crust, creating accommodation space for peat formation (Edwards, 2009), presents an explanation for pan origin worth examining. This study hypothesizes that sagging of the surface of the Earth due to deep weathering of rock, can lead to pan formation.

Pans occur on the African Erosion Surface in the vicinity of Grahamstown, South Africa, and the reasons for their existence are poorly understood. Although Allan *et al*. (1995) did not consider bedrock type to be a reliable indicator of pan distribution, Dwyka tillite on the African Erosion Surface seems to be associated with the formation of pans in the vicinity of Grahamstown. Furthermore, it seems likely that weathering from parent material to produce kaolinite could be associated with volume loss. The African Erosion Surface in the vicinity of Grahamstown is capped by a layer of highly resistant silcrete, which has developed as a result of deep chemical weathering of the Dwyka tillite.

Chemical weathering involves the breakdown of basic constituents of a rock by interaction with water (hydrolysis) and acidic or oxidising agents to release ions. Over extended time periods these ions will form new minerals that are more stable under surface conditions than their parent minerals.

The silcrete formed as a result of chemical weathering of the Dwyka Tillite forms a gently undulating plateau which has inhibited the degree of erosion in the surrounding landscape. This

study aims to contribute to our understanding of pan origins through the development of a conceptual model of deep weathering of bedrock, which over extended time periods, leads to subsidence of the Earth's crust and ultimately pan formation.

1.2 Aim

The aim of this study is to examine the role of mass loss and volume reduction due to deep weathering as a possible factor contributing to the origin of pans on the African Erosion Surface in the area around Grahamstown in the Eastern Cape, South Africa.

1.3 Objectives

In order to achieve the aim a number of objectives have been identified.

1. The morphology of these pans must be ascertained.
2. Compare the geochemical properties of the material beneath and adjacent to the endorheic basin to each other and to the parent lithological material to determine likely gains and losses of elements.
3. Determine the mineralogy of the endorheic basin and the surrounding parent material and calculate density and volume changes.
4. Determine the nature of surface water and groundwater interaction
5. Develop a conceptual model of the origin and evolution of pans on the African Erosion Surface near Grahamstown which can be integrated with existing models of wetland origin.

Chapter 2: Literature Review

2.1 Wetlands of South Africa

A wetland as defined by South Africa's National Water Act, is "land which is transitional between terrestrial and aquatic systems where the water table is usually at or near the surface, or the land is periodically covered with shallow water, and which in normal circumstances supports or would support vegetation typically adapted to life in saturated soils." Wetlands occupy 4-6 % of the global land surface and contain highly diverse sedimentological and geomorphological features (Tooth and McCarthy, 2007). The study of wetlands currently is increasingly interdisciplinary, mainly a combination of ecological, hydrological, and biological sciences, with the study of the geomorphological and sedimentological features and impacts being limited and poorly understood (Tooth and McCarthy, 2007). Hydrological factors have the largest control over the formation, size and persistence of a wetland (Ellery *et al.,* 2009). The hydrological factors are influenced by factors such as climate, geology and tectonics, and geomorphology of the area (Ellery *et al.,* 2009).

Dryland is collective and refers to areas that range from sub-humid to hyper-arid environments, and makes up around 50 % of the global land surface (Tooth and McCarthy, 2007). In the drylands especially, there is a lack of understanding with regard to the geomorphological and sedimentological features associated with wetlands (Tooth and McCarthy, 2007). Most of southern Africa falls into the category of Dryland, but there are regions that are more humid along the southern and eastern margins of the subcontinent (Tooth and McCarthy, 2007).

As outlined by Tooth and McCarthy (2007), the limitations of excluding geomorphological and geological factors means that there is no synthetic framework for understanding 1) controls on distribution or location, 2) processes involved in development, 3) when their forms developed to the present day morphology and how rapidly they are changing, 4) their sensitivity to changes in their environment, and 5) their likely trajectory of development in the future.

2.2   Pans

2.2.1 Defining a pan

The terminology for semi-arid depression wetlands varies considerably from country to country, reflecting its parochial nature. Certain terms such as pans and playas are interchangeable, although authors tend to prefer to use the term pan when describing a small basin which has formed through arid geomorphologic processes (as opposed to geological processes). The term playa is generally used for a basin with a saline evaporite surface (Shaw and Thomas, 1997), historically with a coastal affiliation since the word *playa* means shore in Spanish (Rosen, 1994). In the Sahara for example, terms such as *sebkra, sebjet, sebchet, sebkha, sebkhah, sebcha, zahrez, chott,* and *garaet* are used in different areas to describe similar features (Cooke and Warren, 1973). Because the terminology is so area specific, there have been attempts to assign diagnostic characteristics to a specific term, such as limiting the term Sebkhah (a generally Arabian term) to describe saline flats which occur in coastal areas above the level of high tide. The attempt to clarify such terms has only led to confusion as authors from different countries have preferred their own countries' terminology or simply do not adhere to the revised definitions (Shaw and Thomas, 1997). By using the terms interchangeably, a pan can thus be defined as a basin located in an arid to semi-arid region, which varies widely in size and origin, and generally exists above the present day water table but is subject to irregular and uncommon surface water inundation. Evaporitic sediments along the base and margin of pans are also common (Shaw and Thomas, 1997).

The most common characteristic of pans is that they occur in depressions or closed basins (Shaw and Thomas, 1997). Pans are generally sub-circular or kidney shaped land features, although linear pans can occur when the morphology is controlled by the surrounding landforms such as linear dunes (Shaw 1988). A common feature of all pans is a flat basin floor and the depression itself may be 20 to 30 meters below the surrounding land surface. Le Roux (1978) has noted that, in the Free State (South Africa), the long axis of a pan develops perpendicular to the prevailing wind direction; an observation supported by Goudie and Thomas (1985).

South African pans virtually all occur on Kalahari Group and Karoo Supergroup lithologies. The Ecca Shales and the Dwyka tillites, plus some of the sandstones and mudstones in these Groups, are prevalent hosts of pans in South Africa (Shaw, 1988). Shaw (1988), in agreement with several other authors that he cites, has suggested that preferential weathering of ancient groundwater flow paths is related to the formation of pans on the Kalahari sub-surface. This hypothesis of deep weathering of groundwater flow paths can be applied to shallower flow paths in, for example, ancient rivers. Features common to pans are summarised in Table 1, including their relationships with topography, hydrology, permanence of inundation, characteristics of the water balance and vegetation (Shaw and Thomas 1997).

Table 1: Summary of the common characteristics of pans as taken from Shaw and Thomas (1997)

Characteristics common across pans
Occur in topographic depressions
Absence of surface outflows
Ephemeral flooding of basin
Evaporation greatly exceeds water input (negative water budget)
Basin floor is usually flat
Have either vegetation free surfaces, or distinct associations with vegetation

Features that differ between pans (Table 2) include their mode of origin, size, their overall morphology, regularity of flooding, relative contributions of surface and groundwater, parent geology and nature of sedimentary fill.

The precipitation of evaporites on the surface of pans and the occurrence of calcrete alteration products at depth is not uncommon in pans (Shaw, 1988). Calcrete can often form ridges which can extend hundreds of metres beyond the pan. Silcrete layers or nodules commonly occur within the calcrete, either as precipitation or calcium replacement products (Shaw, 1988). The most common salts are calcium sulphates, sodium chloride, and sodium carbonates (Shaw, 1988).

Table 2: Summary of variable characteristics in pans (adapted from Shaw and Thomas, 1994).

Variable characteristics of pans
1. Origin
2. Size
3. Morphology
4. Regularity of flooding of basin
5. Relative importance of surface water and groundwater
6. Sedimentology and bedrock geology

2.2.2 Pan distribution

Pans have been identified worldwide in arid and semi-arid landscapes (Shaw and Thomas, 1997). In Africa, pans have been identified in the Sahara and Kalahari, and the regions surrounding them (Shaw and Thomas, 1997). Globally there are certain areas which are notable hosts of pans, namely southern Africa, central Africa, central North America, the Pampas and Pantanal of South America, southern and western Australia, western Siberia, and Manchuria in China (Goudie and Wells, 1995). Pans in southern Africa occur over a surprisingly wide range of climatic and geological settings, from the semi-arid Kalahari of the Northern Cape, southern Botswana and Free State, to the moist Highveld of Mpumalanga (Goudie & Thomas 1985; Rogers, 1997; Dini *et al.,* 1998). This review will focus on pan distribution in South Africa.

In certain parts of southern Africa the distribution of pans seems random (Shaw, 1988), but there are four main factors which influence pan distribution: drainage, slope gradient, bedrock, and climate (Le Roux, 1978). With the exception of the Highveld of Mpumalanga, pans in southern Africa are generally distributed in areas with a mean annual rainfall less than 500 mm and a mean annual free surface evaporation of more than 1000 mm (Goudie and Wells, 1995; Figure 1). Pans are distributed across many of the biomes, being particularly common in the grassland, Nama Karoo and Desert biomes (Allan *et al.,* 1995). The highest concentrations of pans are found in the Northern Cape, the Free State, and the southern Mpumalanga Highveld (Goudie and Wells, 1995; Allan *et al.,* 1995).
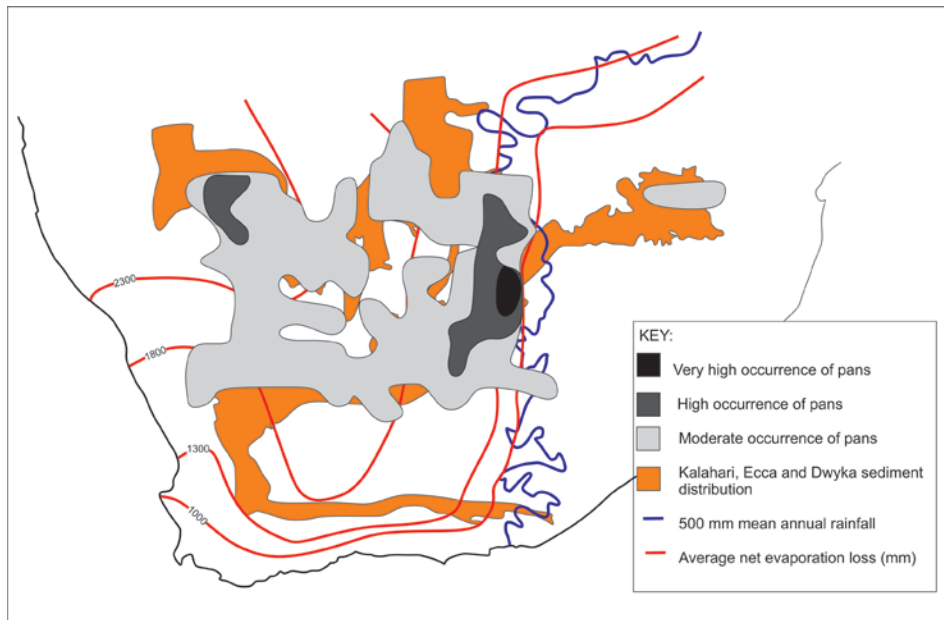
Figure 1: Pan distribution in southern Africa. Due to the scale of the map most small pans are not shown, but when they are included the distribution pattern however, remains the same (adapted from Goudie and Wells, 1995).

The majority of pans are located on, but are not confined to shales (Dwyka and Ecca) and unconsolidated sediments. Other common bedrock types include Dwyka tillite and dolerite (Allan *et al*., 1995). Allan *et al.* (1995) suggests that bedrock is not a clear indicator of pan distribution. Areas with limited integrated drainage and a mean slope below one degree contain the highest concentration of pans (Le Roux, 1978). Additionally some pans (such as in the Kalahari) are found in association with landforms that appear to have contributed to their development (Shaw, 1988). These are landforms that impede drainage (dunes or ridges), or preferentially direct the flow of groundwater (fossil valley) (Shaw, 1988).

2.2.3 Current understanding of the origin of pans

Goudie and Thomas (1985) created a model for pan origin based on wind deflation of animal watering areas where vegetation has been removed by animal activity (Figure 2). In this model animals concentrate around areas with available surface water and essential salts. This generally leads to localised overgrazing. Where localised overgrazing occurs in areas of low precipitation and generally limited vegetation cover, the land surface is left highly susceptible to deflation. The second factor of great importance in the Goudie and Thomas (1985) model is the lack of integrated drainage which limits fluvial erosion and sedimentation

8

and is a controlling factor in evaporite formation. In addition, low relief is vitally important as pans tend to develop in low energy environments.
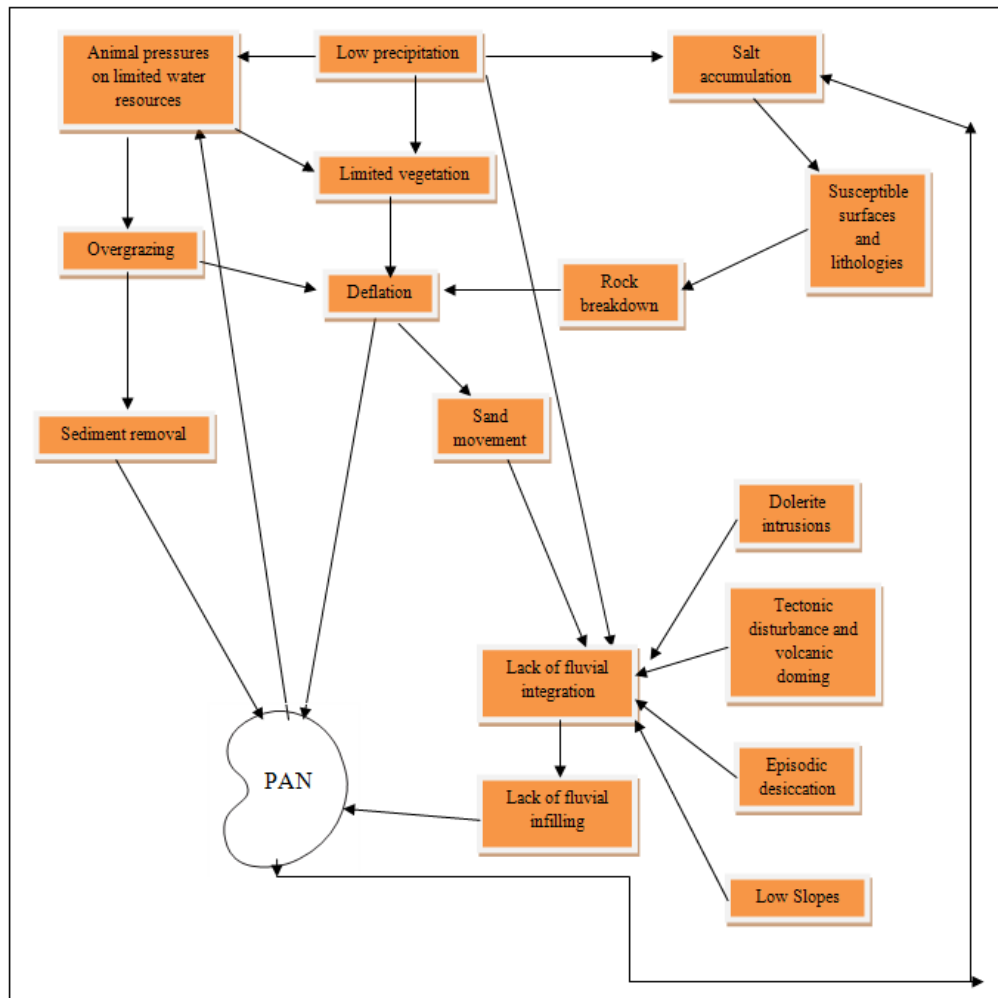
Figure 2: The pan origin model as developed and described by Goudie and Thomas (1985)

Shaw and Thomas (1997) recognized three main contributing factors which can act independently or in combination to create a pan; structural controls, erosional controls, and ponding controls.

Structural controls: Down-warping and faulting can create major basins such as those found in the Basin and Range in the USA. Rock fracturing may also influence pan genesis by creating flow pathways for groundwater and delimiting the extent of the local drainage

basin. Intrusions may also act as barriers to water flow, influencing the development patterns of a drainage system.

Erosional controls: The role of deflation in pan origins has already been discussed in Goudie and Thomas's (1985) model. Deflation requires that (a) the environment is arid enough for effective aeolian erosion, and (b) the surface is susceptible to deflation in terms of a lack of vegetation and material susceptibility. Deep weathering plays an important role as material is removed in solution during chemical weathering. Of importance in areas with dolomitic and limestone lithologies is karstic solution, where a pit or depression can form from the decarbonisation of the lithologies by a suitable fluid agent (be it groundwater or hydrothermal fluids).

Ponding controls: The most notable of these include linear depressions between sand dunes, back-ponding in a relict channel by disruption with recent sedimentation, and formation of basins by deposition of sand bars and beaches in coastal areas. Tributary valley and floodplain margin lakes formed by floodplain aggradation, are often referred to as "pans" (Grenfell *et al,*. 2009; Ellery *et al*., 2012), which may not be an entirely appropriate terminology.

A common feature of pans in southern Africa is that they occur on the African erosion surface, an ancient erosion surface that dates back about 65 million years (McCarthy *et al.,* 2007).

2.3   The African Erosion Surface

During the late Jurassic (approx. 170 Ma) there was a change in the tectonic regime from compressive tectonics, which led to the creation of the Karoo Foreland Basin characterized by orogenic loading and unloading events, to extensive tectonics associated with the initiation of the break-up of the supercontinent, Gondwana. At the onset of the Gondwana break-up, the southern African subcontinent is believed to have been elevated with the eastern portion of the continent having the highest terrain due to the proximity of the underlying mantle plume (McCarthy and Rubidge, 2005; Figure 3). Due to rifting and formation of seas along the margin of the continent, a marginal escarpment formed at the edge (McCarthy and Rubidge, 2005; Figure 4). The period following this was particularly humid causing rocks within the interior of the subcontinent to experience leaching (McCarthy and Rubidge, 2005). Three major rivers

created a drainage system in the interior of the subcontinent, the Limpopo River draining the northern regions and flowing to the east coast, the Kalahari River which drained the western interior flowing towards the west, and the Karoo River which flowed to the west and drained the eastern highlands of southern Africa (McCarthy and Rubidge, 2005). These rivers eroded rocks of the Karoo Supergroup, but it is not clear how much material was eroded, although it is recognised to have differed according to location. Deposition of these eroded sediments during the Cretaceous created sequences up to three kilometres thick, forming the Kirkwood and Sundays River Formations (Maud, 1996). This erosional period is, however, believed to have formed what is known as the African Erosion Surface, and cut back the marginal escarpment to what we now know as the Great Escarpment (Maud, 1996; McCarthy and Rubidge, 2005; Figure 5). There were two later periods of uplift (20 Ma and 5 Ma) shown in Figure 6, which created the Post African 1 and Post African 2 erosion surfaces respectively (Maud, 1996), with the Lesotho Highlands and parts of the Cape Fold Mountain existing as the only remnants of the ancient pre-African terrain (Maud, 1996; McCarthy and Rubidge, 2005).
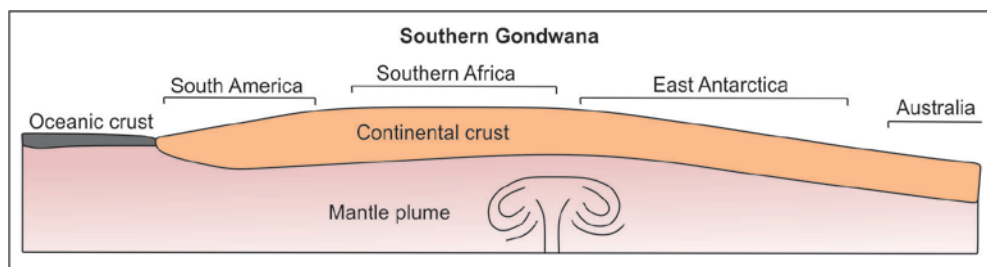
Figure 3: Bulging of the crust of southern Africa due to the onset of a mantle plume beneath the southern African subcontinent approximately 180 Ma. After McCarthy and Rubidge (2005).
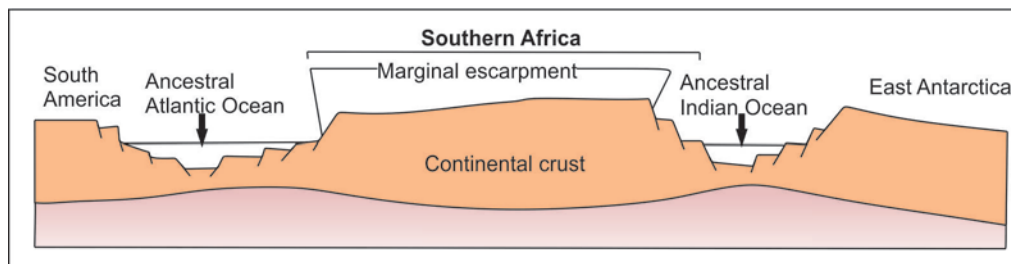
Figure 4: Rifting along the west and east coast of southern Africa thinned the continental crust and forming the proto- Indian and Atlantic Oceans (120 Ma). This was accompanied by the formation of the marginal escarpment. After McCarthy and Rubidge (2005).
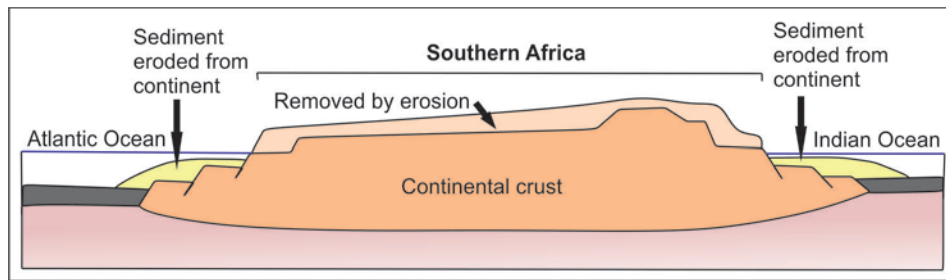
Figure 5: By circa 65 Ma there was creation of oceanic floor spreading centres (Indian and Atlantic Oceans). Intense erosion occurred in the interior of southern Africa, and deposition of these sediments took place on the continental shelf. This process cut back the marginal escarpment. After McCarthy and Rubidge (2005).
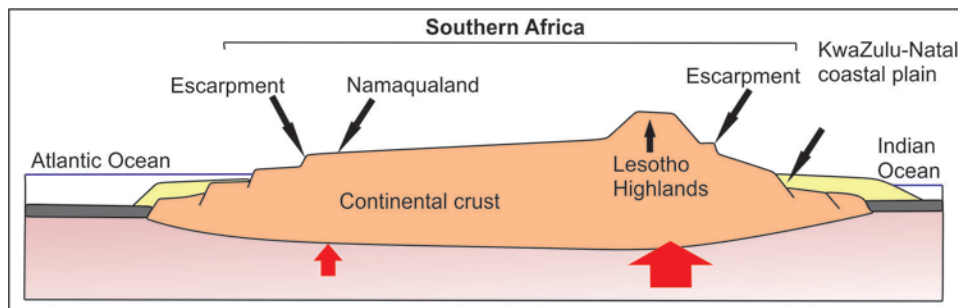
Figure 6: At about 20 Ma and five 5 Ma, there where episodes of uplift and tilting of the southern African subcontinent towards the west, this which created more recent erosion surfaces, however the major features of the subcontinent remained. After McCarthy and Rubidge (2005).

2.4   Chemical weathering

Weathering is a term describing the physical and chemical alteration of minerals or rocks near or at the surface of the earth (Birkeland 1984). Chemical weathering involves reactions caused by acidic or oxidizing agents (water, CO_2, O_2, and other chemical agents) interacting with rocks or minerals, resulting in their breakdown and release of constituents such as dissolved ions (Schlesinger, 1996; Yatsu, 1988) by the consumption of the acidic agent or production of alkalinity (Olsson and Melkerud, 2000). Weathering is a vital process in pedogenesis, and for the supply of nutrients to the biosphere, precipitation of secondary minerals, and acts as a control in the pH of soil (Olsson and Melkerud, 2000). Rocks are weathered according to their composition, texture, and the biogeochemical environment (pH and Eh) prevalent in the region of occurrence (Carroll, 1970), and is essentially governed by the laws of thermodynamics (Yatsu, 1988).

Chemical weathering consists of five main processes (Figure 7), which Krzic *et al.* (2004) summarised with useful examples demonstrating the products of these processes:

1. Hydration: An intact water molecule binds to a mineral. For example, hematite is transformed to ferrihydrate.

Equation 1: Hydration of hematite

$$5Fe_2O_3 + 9H_2O \xrightarrow{Hydration} Fe_{10}O_{15} \cdot 9H_2O$$
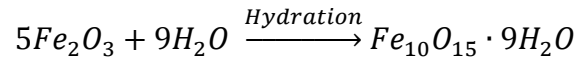
2. Hydrolysis: A water molecule splits into hydrogen and hydroxyl components. The hydrogen replaces a cation in a mineral structure. For example, orthoclase is transformed to kaolinite.

Equation 2: Hydrolysis of kaolinite

$$KAlSi_2O_8 + H_2O \xleftrightarrow{Hydrolysis} HAlSi_2O_8 + K^+ + OH^-$$
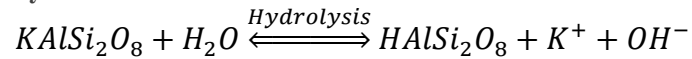
3. Dissolution: A solution is formed when water dissolves minerals through hydration of ions until they are completely isolated from each other and surrounded by water molecules. For example, the dissolution of gypsum.

Equation 3: Dissolution of gypsum

$$CaSO_4 \cdot 2H_2O + 2H_2O \xleftrightarrow{Dissolution} Ca^{2+} + SO_4^{2-} + 4H_2O$$
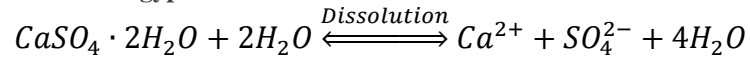
4. Carbonation: The presence of acids produced from CO_2 accelerates chemical weathering by increasing the activity of hydrogen ions in water. For example, when carbon dioxide is dissolved in water it produces carbonic acid (H_2CO_3), which accelerates dissolution of calcite into calcium bicarbonate.

Equation 4: Carbonation resulting in Ca bicarbonate

$$CO_2 + H_2O \xleftrightarrow{\hspace{1cm}} H_2CO_3$$

$$H_2CO_3 + CaCO_3 \xleftrightarrow{Carbonation} Ca(HCO_3)_2 \text{ (aq)}$$
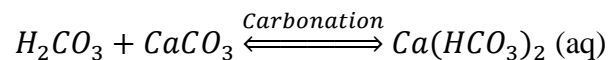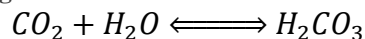
5. Oxidation-reduction: Elements Fe, Mn, and S can exist in a divalent or trivalent form, and hence are susceptible to oxidation-reduction reactions. For example, the oxidation-reduction reaction of pyrite during acid mine drainage (Blodau, 2006).

Equation 5: Oxidation-reduction of pyrite (Blodau, 2006)

$$2FeS_2 + 7O_2 + 2H_2O = 2Fe^{2+}(aq) + 4SO_4^{2-}(aq) + 4H^+(aq)$$

		Process	Response
Climatic function → Physical		Crystallization	Disintegration
		Thermal process	Volume change
		Wetting and drying	Grain-size change
Lithological function → Chemical		Hydration	Decompaction
		Hydrolysis	Recombination
		Solution	Cation exchange
		Oxidation-reduction	Leaching
		Carbonation	Dissolved ions
		Chelation	
Biological function Biological		Growth	Accumulation
		Decomposition	Mineralization
		Burrowing	Pulverization
		Bio-chemical change	Nutrient uptake

Figure 7: Processes involved in Weathering, with particular focus on the processes of chemical weathering (Krzic *et al*., 2004)

2.4.1 Water (H$_2$O) as an agent of chemical weathering

The water involved in chemical weathering is supplied mainly by rain, which percolates through joints and fractures to the site of chemical weathering or is available through the water table (Carroll, 1970). Water plays the important role of acting as solvent and chemical reactant. Virtually all chemical weathering processes need water to occur (Yatsu, 1988), without which only physical disintegration and small amounts of oxidation could occur (Carroll, 1970). Water consists of one oxygen atom covalently bonded to two hydrogen atoms and is the most abundant electrolyte, although weak in nature. The dissociation of water occurs with this reaction:

Equation 6: Dissociation of water

$$2H_2O \leftrightarrow H_3O^+ + OH^-$$
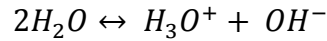
which is simply abbreviated to

$$H_2O \leftrightarrow H^+ + OH^-$$
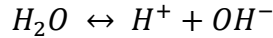
Rainwater contains relatively few dissolved solutes such that the composition of rainwater is more-or-less seasonally constant for a given geological location (Carroll, 1970). Rainwater contains a mixture of cations and anions which act to make it an electrolyte. Ammonia and nitrogen compounds are always present in rainwater (Carroll, 1970). Solutes such as Na, Mg, K, Ca, Cl, bicarbonate, and sulphate ions are present as ions in rainwater, and minor constituents include iodine, bromine, boron, iron, Al, and Si (Carroll, 1970). Dust is also usually present in varying amounts depending on factors such as climate and, in modern times, industry and population (pollution) factors (Carroll, 1970). The sources of these ions in rainwater range from volcanic emanations to vegetation to oceans and lakes. The amount of water available controls the amount of chemical weathering that can take place (Carroll, 1970). Factors such as water drainage patterns and position of the water table also play a vital role in influencing the rate and degree of weathering. As described by Carroll (1970) there are four types of water involved in chemical weathering:

1. Gravitational: this water percolates downwards and drains leached ions.
2. Capillary: this water is held by capillaric force in pores.
3. Hygroscopic: this is water that is held around a particle as a thin film due to ionic bonding.
4. Combined: this water has been incorporated in a crystal lattice, and can only be removed by the alteration of a mineral into another mineral or through alteration of the crystal lattice.

Hygroscopic and capillary water act as the medium for ion exchange. Rainwater's composition is changed through interaction with hygroscopic and capillary water already present in the ground. Thus the pH of the water which will be available for chemical weathering is determined by the original pH of the rainwater and the interaction with the hygroscopic and capillary water already present in the system. The pH of water is a vital factor, as chemical weathering typically takes place in a mildly acidic medium. The process of hydrolysis will in

turn change the pH of the water and the composition of the material through which the water is passing will therefore directly influence the composition of drained water. In other words, water which has passed through igneous rocks will differ from water which has passed through metamorphic or sedimentary rocks. Since pH is so vital during the process of chemical weathering it is necessary to discuss the role of acids involved in chemical weathering.

2.4.2 The role of hydrolysis

Hydrolysis generally refers to the breakdown of chemical bonds through the addition of water (Carroll, 1970). At least 75 % of the earth's surface is made up of silicate minerals (Nahon, 1991). Aluminosilicates make up by far the largest proportion of the silicate minerals present in the earth's crust; as such both silicon and aluminium play important roles in the provision of reacting salts in hydrolysis. Aluminium is particularly important as, like water, it is amphoteric – meaning that it can lend itself to being an acid or a base (Carroll, 1970). Water, whose importance in chemical weathering has already been stressed in this chapter, is the causative reagent of hydrolysis. The pH of the fluid phase determines whether H^+ or OH^- remains to react with minerals. The chemical composition of rocks reacts to reach thermodynamic equilibrium; thus, as conditions change, such as pressure (due to erosion or unearthing of rocks) and temperature (due to changes in climate), the rock will need to re-equilibrate (Carroll, 1970). It does this through the chemical breakdown of minerals to form new minerals which are stable under the new conditions. In 1938, Goldich (as cited in Carroll, 1970) constructed a series for the stability of minerals during weathering (Figure 8). Understanding this series is rather simple, as it is the minerals with weak bonds which will weather first and the minerals with strong bonds that will weather last. The hydrolysis reaction of a mineral is called the abrasion pH (Carroll, 1970), and it essentially describes what will happen to the pH of the reagent fluid (the water in contact with the weathering minerals) when a mineral is weathered by hydrolysis. The abrasion pH of a mineral can be tested and understood through crushing a mineral into a fine power and adding this powder to water. The pH of the water will change accordingly; for example with an alkali mineral, alkali cations are released and the pH will increase. This new pH will therefore determine how the reagent fluid interacts with the remaining rock forming minerals.
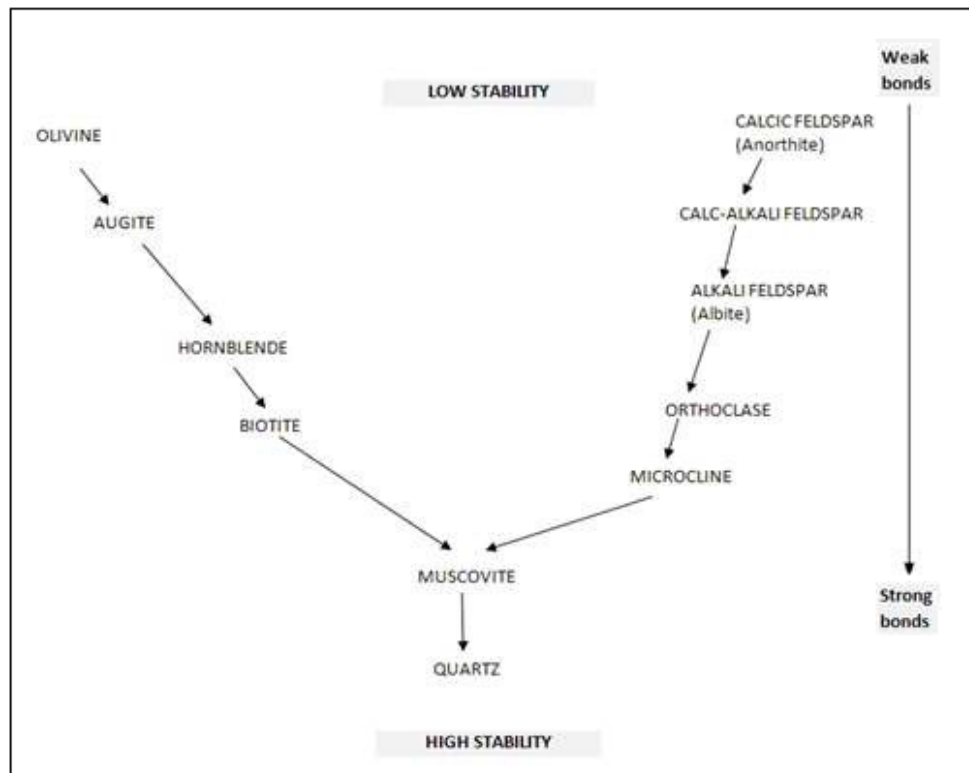
Figure 8: A mineral weathering series as described by Goldich (1938).

The hydrolyzation of minerals during weathering is complicated by the properties of both silicon and aluminium. Figure 9 shows the solubility of crystallizing quartz, amorphous quartz, and aluminium, in relation to variations in pH. Between a pH of 4 and 8.5 aluminium is only very slightly soluble; however, quartz has a solubility of approximately 6ppm over the same pH range, which increases above a pH of 9. It is therefore slightly soluble under most weathering conditions but, in small amounts, amorphous silica is 20 times more soluble than quartz. These relative solubilities of quartz and aluminium mean that, under normal circumstances (pH between 6 and 8) and given sufficient time, weathering will slowly decrease the amount of silica relative to aluminium in the weathering rock material (Carroll, 1970). This accumulation can be most easily recognised in well-formed soils that haven't been eroded (Carroll, 1970). In the acidic solutions a cationic form of aluminium exists as $Al(OH)_2^+$, whereas in basic solutions an anionic form of aluminium exists as $AL(OH)_4^-$ (Carroll, 1970). Reactions in the acid range of solubility for aluminium occur very slowly; if the pH rises dissolved species of

Al^+ and OH^- will form, if the concentration of OH^- is sufficient then $Al(OH)_4$ will precipitate, and if the fluid becomes alkaline, the precipitate will be redissolved. For the most part the pH during weathering stays below 6.7, which is the isoelectric point of aluminium (Figure 9). As aluminium almost always accumulates, it can therefore be said to be immobile during the chemical weathering process.
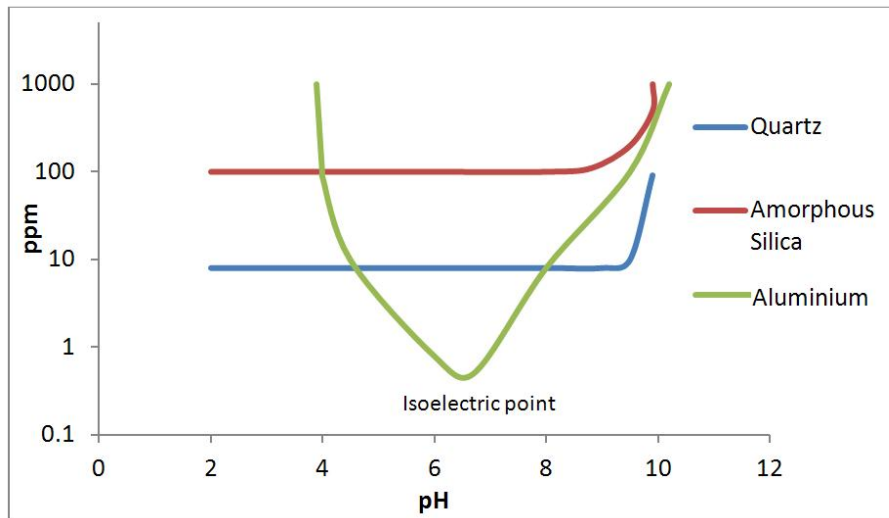
Figure 9: Solubility curves of silica and aluminium with variation in pH (after Carroll, 1970).

During hydrolysis most elements can be categorized as behaving as either mobile or immobile. During chemical weathering of granitic and basaltic rocks, Si, Mg, Ca, and Na are leached, Al and Ti accumulate, and Fe and K behave in a more complicated way (Harnois, 1988). Iron exists naturally in rocks in two oxidation states, ferric iron (Fe^{3+}) and ferrous iron (Fe^{2+}). Ferric iron is not as soluble as ferrous iron, and the proportion of iron left behind depends upon the redox conditions during weathering (Harnois, 1988). Potassium is usually leached, but once it is in solution K^+ can, through ion exchange, substitute Na^+ or Ca^+ in clays to form K-minerals (Harnois, 1988).

The breakdown of a given mineral depends not only on the elements which are present in the mineral but also the relative amounts of each element. In feldspars for example, the reagent fluid forms a thin film around the mineral and potassium is replaced by H^+ ions,

which deforms the crystal lattice. In plagioclase feldspar however, potassium is the cation that is present in the smallest abundance and it is removed preferentially.

During hydrolysis, the first process is the hydration of minerals. In this early stage of hydrolysis there is generally no change in the mineral structure. The hydration potential of a mineral is a function of its ionic charge such that the absorption of water by the mineral increases with increasing ionic charge. A mineral such as ferric oxide can readily hydrate whereas quartz cannot absorb water (Carroll, 1970). Hydration is commonly accompanied by carbonation.

2.4.3 Ca, Mg, K and Na adsorption

The most common cations that will be present in solution are Ca, Mg, K, and Na. Cations are able to displace and replace each other during interaction (Polynov, 1937). The adsorption of such elements depends upon their "energies of adsorption in the adsorption complex" (Polynov, 1937; pg 134). For the elements of interest here, the series for adsorption is as follows (Polynov, 1937):

Ca > Mg > K > Na
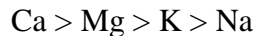
This means that if all four elements are present in solution in the same abundance then Ca will be adsorbed first, followed by Mg, then potassium and lastly Na (Polynov, 1937). Adsorbed Ca is found in virtually all soils from tropical to glacial and even desert. The stability of a complex containing such elements is not as simple as saying that Ca is more stable in a complex than Mg, which in turn is more stable than potassium and so on. For example, although Ca will be adsorbed before Mg, once Mg has been adsorbed into a complex, it is more stable than Ca (Polynov, 1937). Exchangeable cations are cations which will readably be displaced by other cations due to the mass ion effect (Krzic *et al.,* 2004). Cation exchange is rapid, reversible, and occurs stoichiometrically (Krzic *et al.,* 2004). When one determines the composition of exchangeable bases, it is likely that the alkali elements are present in very small amounts, which is especially true for potassium (Polynov, 1937). In a simplified system containing only potassium and sodium cations and clay colloids, exchange would occur as seen in Equation 7:

Equation 7: Cation exchange of Na and K with a clay colloid as the exchange site (Polynov, 1937)

$$KClay + Na^+ \leftrightharpoons K^+ + NaClay$$
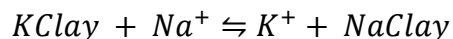
The probability that K^+ will be displaced by Na^+ increases as the amount of Na available in solution increases. If Na^+ becomes extremely abundant it is very likely that virtually all the K^+ cations will be displaced, which is known as the mass ion effect (Krzic *et al.,* 2004).

2.4.4 Chemical weathering indices and measurement

Understanding the processes involved in chemical weathering is important, but there also needs to be a system that one can use to quantify the relative amounts of weathering that exist in a system. Since the beginning of the 20th century there have been over 30 weathering indices proposed (Duzgoren-Aydin *et al.,* 2002). These chemical weathering indices are either based on assumptions or have criteria for applicability of the index. The majority of indices have been proposed for felsic to intermediate rocks that are weathered under well-drained conditions. Duzgoren-Aydin *et al.* (2002) and Price and Velbel (2003) published results that assessed or re-assessed the use of various chemical weathering indices. The former study was more comprehensive in terms of the number of indices discussed. Duzgoren-Aydin *et al.* (2002) classified indices into groups based on their weathering calculation method (Figure 10). Indices can be grouped into methods based on either mineral compositions or whole rock compositions; indices based on calculations of whole rock compositions are far more common, and can be subgrouped into non-ratio indices, atomic proportion indices, weight percent indices, and molecular ratio indices. A common feature of many of the indices is the use of mobile to immobile ratios.
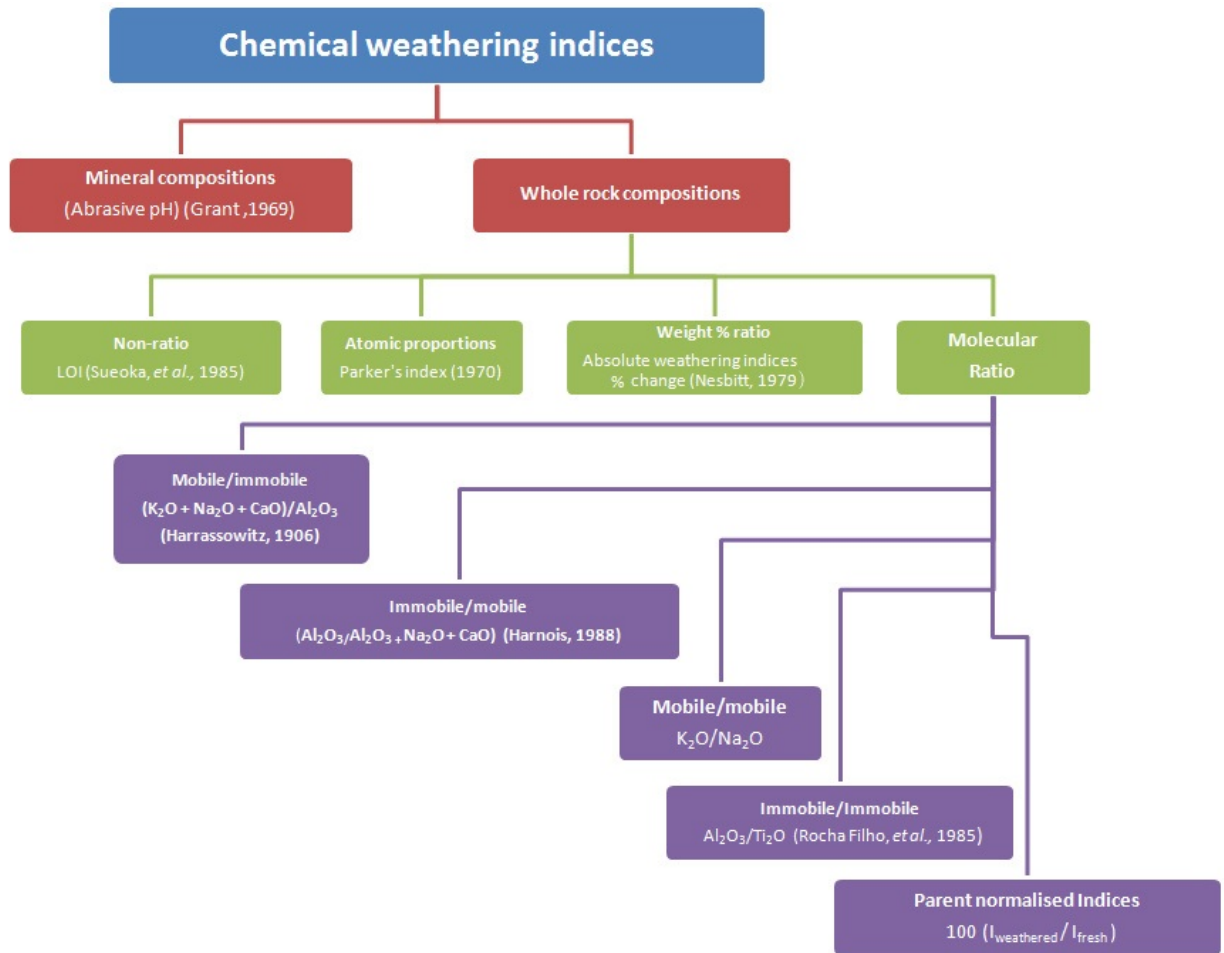
Figure 10: Grouping of chemical weathering indices (after Duzgoren-Aydin *et al*., 2002).

The main assumption in the formulation of these indices is that element behaviour is purely a function of the degree of weathering (Duzgoren-Aydin *et al.,* 2002). There are three more assumptions that are vitally important to the majority of these indices: a) certain major elements and compounds such as Al_2O_3, TiO_2, and Fe_2O_3 are immobile during weathering and therefore relative abundances increase during weathering, b) Si_2O, Na_2O, CaO, MgO, and K_2O are considered mobile and therefore relative abundances decrease during weathering, and c) the amount of material lost on ignition (LOI or loss-on-ignition) increases with weathering (Duzgoren-Aydin *et al.,* 2002). All of the indices reviewed by Duzgoren-Aydin *et al.* (2002) and Price and Velbel (2003) are based on whole rock major element compositions. It is recommended that chemical weathering indices are used in addition to petrographical and mineralogical studies because of the variance in

microenvironmental conditions such as pH and leaching, which can vary significantly over a weathering profile (Duzgoren-Aydin *et al.,* 2002; Bahlburg and Dobrzinski, 2011).

There are three candidates that have been chosen as potential indices for this study.

2.4.4.1 The chemical index of alteration (CIA)

The Chemical Index of Alteration (CIA) is one of the most widely used proxies for weathering (Bahlburg and Dobrzinski, 2011; Li and Yang, 2010). It is interpreted as a measure of the extent of feldspar conversion into kaolinite and other clays (Nesbitt and Young, 1984, 1989; Fredo *et al.,* 1995; and Maynard *et al.,* 1995; cited in Price and Verbel, 2002). Nesbitt and Young (1982) formulated the CIA through work on the reconstruction of paleoclimate from sediments dating to the Early Proterozoic, which form part of the Hurion Supergroup in Canada. The CIA formula is based on the ratio of the immobile element Al_2O_3 to the sum of Al_2O_3 and the more mobile oxides CaO, Na_2O and K_2O (Equation 8).

Equation 8: The CIA as developed by Nesbitt and Young (1982)

$$CIA := 100 \times \frac{Al_2O_3}{(Al_2O_3 + CaO + Na_2O + K_2O)}$$

Shao *et al.* (2012) and Li and Yang (2010) both express caution about using the CIA to determine instantaneous chemical weathering results, but they suggest that the CIA does provide a picture of the integrated long-term weathering history.

2.4.4.2 The Chemical Index of Weathering (CIW)

Harnios (1988) cautioned against the use of the CIA in all environments as it incorporates K as one of the mobile elements factored into the equation. Harnois (1988) believed that because K is a commonly leached element in weathering systems, it should not be included in the calculation of weathering intensity. As a result the CIW (Chemical Index of Weathering) method was introduced. It is similar to the CIA method with the modification that K_2O is omitted as it can be either leached or accumulated (Equation 9). Harnois (1988) believed that the CIW is a superior index because it only incorporates a few elements whose geochemical behaviour is consistent during weathering.

Equation 9: The CIW as developed by Harnois (1988)

$$CIW = 100 \times \frac{Al_2O_3}{(Al_2O_3 + CaO + Na_2O)}$$

2.4.4.3 Parker's Weathering Index (WIP) also known as Parker's Index

Because the breakdown of feldspars into clay minerals and the resultant mobility of elements is a major process in chemical weathering, Parker (1970) attempted to mirror changes in Na, K, Ca, and Mg with weathering, and came up with the weathering index (WIP) (Equation 10).

Equation 10: The WIP as developed by Parker (1970). Calculations are done with molecular proportions.

$$WIP = \left(\frac{2Na_2O}{0.35} + \frac{2K_2O}{0.25} + \frac{MgO}{0.9} + \frac{CaO}{0.7}\right) \times 10$$

The WIP has been criticised for only containing mobile elements, which has potential limitations in strong weathering profiles such as bauxites (Shao *et al.,* 2012; Price and Verbel, 2003) and Balhburg and Dobrzinski (2011) believed that this limited the WIP from detecting relative compositional changes in mineral phases during weathering.

A comparison of these weathering indices is provided in Table 3, with an emphasis on documenting the assumptions that have been made with respect to important characteristics of weathering, and also comparing the indices to each other. The table notes assumptions based on the mobilities of the elements potassium and aluminium, and how to understand an index value in terms of degree of weathering. Also outlined is how consistent an index has been when applied to various well known sites of chemical weathering.

Table 3: Summary of important distinctions between the CIA, CIW, and the WIP.

Index	Assumptions or conditions	Correlation with studies	K behaviour	Allows Al Mobility	Ideal weathered value	Ideal fresh value
CIA	- Based on the molecular ratio of immobile/mobile elements. - Ca, Na, and K must decrease as degree of weathering increases (Nesbitt and Young, 1982).	- Good correlation with Bahlburg and Dobrzinski (2011) - Good correlation with Shao *et al.* (2012) - - Fair correlation with Price and Verbel (2003) - Fair to good correlations with Li and Yang (2010)	Mobile	No	100	≤ 50
CIW	- Based on the molecular ratio of immobile/mobile elements. - K is considered to have inconsistent geochemical behaviour and is therefore not included as a mobile element (Harnois, 1988).	- Bad correlation with Duzgoren-Aydin *et al.,* (2002). - Fair to bad correlation with Price and Verbel (2003)	Leached	No	100	≤ 50
WIP	- Atomic proportions of mobile elements are used (Parker, 1970). - Hydrolysis is the main agent of weathering (Parker, 1970). - Based on bond strength and mobility's of elements (Parker, 1970). Based on whole rock CaO not only silicate CaO (Bahlburg and Dobrzinski, 2011). No consideration of immobile phases.	- Good correlation with Duzgoren-Aydin *et al.* (2002). - Good correlation with Shao *et al.* (2012) Very Good correlation with Price and Verbel (2003) - Fair correlation with Bahlburg and Dobrzinski (2011)	Mobile	Yes	0	100

2.5 The geomorphic significance of silcrete

The term silcrete was first used in 1902 by Lamplugh (cited in Nash and Ullyott, 2007) to describe silica accumulations at or near the surface of the earth in or replacing soil, sediment, rock or weathered material (Nash and Ullyott, 2007). Silcretes occur commonly in Australia, southern Africa, and Western Europe. The majority of silcretes are remnants of pre-existing geological features (Summerfield, 1983). Silcrete can exist in numerous forms, but most commonly it occurs in a massive brittle form or as nodules of hard silica cemented sand with conchoidal fractures. Very hard fine-grained cherty varieties also exist.

2.5.1 Silcrete classification

The classification of silcretes has changed a lot since the first sub-division of silcretes by Goudie in 1973 (cited in Nash and Ullyott, 2007). Nash and Ullyott (2007) outline attempts made by various authors to classify silcretes, which have been summarized in Table 4. As can be seen, silcretes vary considerably. There are five well known classification schemes to classify silcretes into groups, each using different criteria based on genetic, macromorphological, or micromorphological features. Due to the wide range of terms used to classify silcretes, there is a lack of consistency in the literature, as silcrete nomenclature is entirely dependent on the classification scheme to which one subscribes. The most comprehensive of these classification schemes was designed by Thiry (1999; as cited in Nash and Ullyott, 2007) and includes criteria based on genetic, macromorphological and micromorphological features.

Table 4: Classification of silcretes by various authors as outlined by Nash and Ullyott (2007)

Author, year	Classification	Notes
Goudie, 1973	Genetic classification of duricrusts	Six types of silcretes classified according to their sub-environment:. 1) Fluvial, 2) Lacustrine, 3) *In situ* models, 4) Capillary rise from groundwater or fluctuation of groundwater, 5) Pedogenic models (i) per ascensum (ii) per descensum, 6) Detrital types of secondary origin
Smale, 1973	Morphological classification of silcrete	Five types of silcretes based on macroappearance, some named after type rock. 1) Terrazzo, 2) Conglomeratic, 3) Albertinia, 4) Opaline/fine grained massive, 5) Quartzitic
Wopfner, 1973, 1978	Matrix (cement) and macromorphological classification	Three groups of silcretes based on matrix (crystalline, cryptocrystalline, or amorphous); habit; and profile: preservation of original textures versus within or below zones of pedogenesis
Summerfield, 1983	Micromorphological classification of silcrete	Classified into 4 groups according to fabric types 1) GS-fabric, 2) F-fabric, 3) M- fabric, 4) C-fabric
Thiry, 1999	Genetic classification of silcrete	An extensive classification scheme that categories silcretes into 3 groups based on macromorphology, host material, fabric/chemistry, and paleoenvironment. 1) Pedogenic silcrete, 2) Groundwater silcrete, 3) Silicification of evaporites

2.5.1.1 The origin of silcrete

Instead of focusing on the complexity of choosing a classification scheme and going into detail on the macro-, micro-, or geomorphological features that can be identified in silcretes across the world, the focus of this section will be on the important factors involved in the formation of silcrete. According to Nash and Ullyot (2007) the three most important factors to take into account when attempting to understand silcrete genesis are a) the source(s) of silica,

b) transportation routes to sites of silicification, and c) factors leading to the precipitation of silica.

2.5.1.2   Silica sources

The silica involved in silcrete genesis can be derived locally from soil and rocks or can be transported from a distance – typically in solution. Irrespective of the source, the weathering of silicate minerals provides the majority of silica in surface- and groundwater. pH is a vital controlling factor affecting the availability of silica as, in very alkaline conditions (above pH 9), the solubility of silica rapidly increases. At low pH, the breakdown of aluminosilicates can increase the concentration of silica in soil. Unless there is intense leaching only a small amount of silica will come directly from dissolution of quartz, unless quartz is amorphous in which case solubility is higher. Although minerals such as feldspars and ferromagnesian minerals are relatively poor in silica, they readily release silica during weathering. An important source of silica is the kaolinisation of feldspars and clay diagenesis. These processes favour low pH conditions where alteration of kaolinites to opaline silica is possible. There are also biological sources of silica, the best know example being diatoms, although phytolithic silica in higher plants is another important source.

2.5.1.3   Silica transfer mechanisms

Silica can be transported by wind or water. Quartz dust, diatoms, sponge spicules and phytoliths can be transported large distances by wind; any other transfer in the environment is a function of dissolved silica in solution. Transfer mechanisms can be lateral or vertical, although transfer is usually a combination of these. Lateral transfers involve movement of silica in rivers and groundwater. Vertical transfers involve movement of silica-bearing soil or groundwater within the vadose zone, by either upward (*per ascensum*) or downward (*per descensum*) movement. As implied, *per ascensum* mechanisms are upward movements by capillary rise, where silica precipitation is controlled by evaporation or the mixing of the silica solution with downward moving waters. It is important to note that silica precipitation due to capillary rise inhibits further capillary rise and therefore can't be responsible for the development of thick silcrete layers. In contrast, *per descensum* is the downward movement of silica by gravitational movement of water in the soil. Silica precipitation is controlled by a number of processes, but as

for *per ascensum,* the precipitation of silcrete inhibits further percolation and limits the thickness of the layer that can form.

2.5.1.4   Silica precipitation

Silica precipitation is a function of the concentration of silica in solution, which is related to the availability of silica, and to a lesser degree the duration of wetting and drying cycles. The more soluble forms of silica will be the first to precipitate out of solution. If a solution is supersaturated with quartz then precipitation can occur without any other changes or mechanisms, as long as the solution moves slowly. In this case, precipitation is more likely if there is a structure around which the quartz can nucleate to initiate deposition. Evaporation is important at surface conditions during the development of pedogenic silcretes. A range of solutes such as Fe^{3+}, Mg^{2+}, Ca^{2+}, and Na^+ can form complexes with silica, which increase its solubility. The destruction of these complexes, however, can trigger precipitation of silica. In highly saline environments complexes of hydrated opaline silica gel can form.

2.6 Synthesis

The widely accepted model of pan development proposed by Goudie and Thomas (1985), which posits deflation that is initiated by animal activity, seems unlikely to apply in an environment where rainfall is non-seasonal and between 600 and 700 mm per annum. An interesting feature of pan distribution in the Grahamstown region of the Eastern Cape is that they are largely restricted to the African Erosion Surface where silcrete is widespread at the surface. Silcrete is not easily deflated as it is a very hard, dense rock, which acts as a blanket covering much of the land surface on the gently rolling African Erosion Surface surrounding Grahamstown. An alternative model to that of Goudie and Thomas (1985) is needed to explain pan origin in this geomorphic and climatic setting. This study proposes that mass and volume loss associated with deep weathering of bedrock is a possible mechanism of pan formation, and supports the notion that pan origin is poorly understood and that there may be more than one suite of processes contributing to their formation.

Chapter 3: Study Area

The study area is in close proximity of the town of Grahamstown in the Eastern Cape of South Africa. There are many minor pans situated in the area but their locations are not well documented in the literature. They are well known locally to host a spectacular lily of the genus Crinum, which dominate the pans in summer following early summer rainfall.

3.1   Geology of Grahamstown

The brief geological description of Grahamstown is sourced from Jacobs *et al*. (2004).

Grahamstown is situated in a syncline trending WNW to ESE (Figure 11). The oldest geological unit in Grahamstown is the Witteberg Group, the youngest group in the Cape Supergroup rocks that date back to 340 Ma.   The Witteberg Group rocks present near Grahamstown can be subdivided into the shales and the sandstones of the Weltevrede Formation, which are found south of Grahamstown. The Weltevrede Formation is overlain by quartz arenites of the Witpoort Formation, which in turn are overlain by shales and minor sandstones of the Lake Mentz Subgroup. The rocks of the Witpoort Formation are found north and south of Grahamstown, and form the high-lying hills surrounding the Grahamstown valley. They also form the base of the Grahamstown peneplain.

There is another subgroup that does not appear on the map shown in Figure 11, the Kommadagga Subgroup, which is found outcropping west of Grahamstown. The Kommadagga consists mainly of shales, minor greywacke and a few arenite sandstone units. Feldspar content increases up the sequence below the base of the Dwyka Group, representing the cooling of the climate during the onset of Dwyka glaciation. The Dwyka Group, the oldest of the Karoo Supergroup rocks, is found in the centre of the Grahamstown syncline unconformably overlying the Witteberg Group rocks. Dwyka Group rocks consist almost entirely of tillite with an argillaceous matrix. Conformably overlying the Dwyka tillite is the Ecca Group, which consists almost entirely of shales. The peneplain of Grahamstown is a horizontal sequence of resistant silcrete which formed penecontemporaneously with the kaolinisation of the Dwyka tillite.
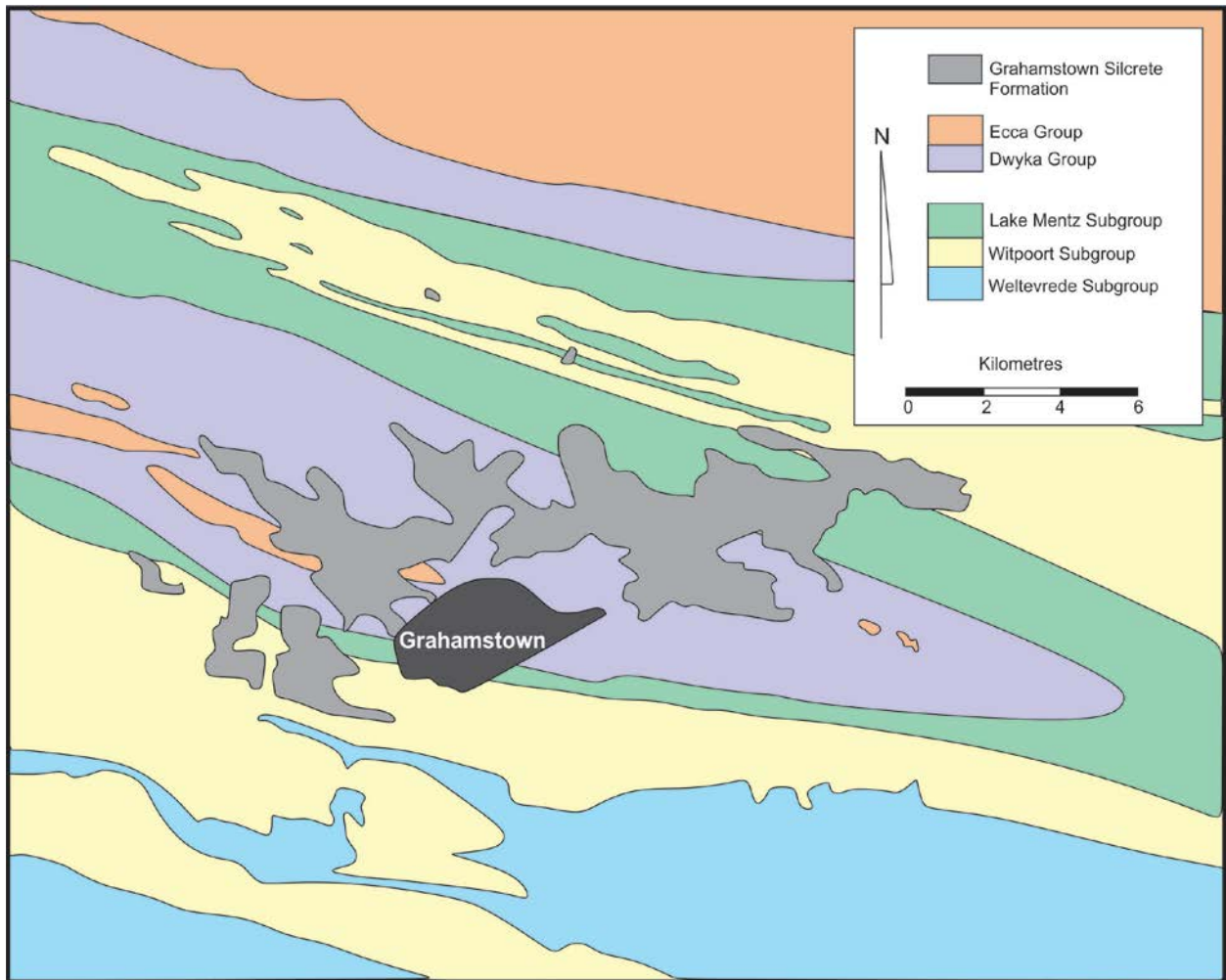
Figure 11: Simplified geological map of the area around Grahamstown (adapted from Jacob *et al*., 2004).

3.1.1 The Dwyka Tillite – Elandsvlei Formation

The lithofacies of the Elandsvlei Formation consists of seven distinct lithologies which are described in Table 5 and illustrated in Figure 12 as summarized by Johnson *et al*. (1997) and Johnson *et al*. (2006). The most abundant facies are the massive diamacite, the massive carbonate-rich diamacite, and the massive daimacite with deformed sandstone bodies. The conglomerate, mudrock, and mudrock with stones facies, typically in the upper half of the profiles (Figure 12), are relatively thin deposits. The Dwyka tillite located at the study area and around Grahamstown, falls into the massive diamacite facies of the Elandsvlei Formation.

Table 5: Lithogical facies of the Elandsvlei formation (Johnson *et al*., 1997)

Lithological Facies	Description
Massive Diamacite Facies	Compacted diamacites with rounded to angular clasts (often showing striations). This rocks formed from melt out in sub-glacial to marine environments.
Massive Diamacite with deformed sandstone bodies	These diamacites differ from the massive diamacite because they contain horizontal and cross-bedded sandstone quartz arenites or quartz wackes, forming irregular deformed sandstone bodies from various environments ranging from esker to tractional fall out deposits.
Massive Carbonate-rich diamacite	These are clast poor diamacites that consist of carbonaceous concretions and carbonate bodies and mudstone lenses.
Stratified Diamacite Facies	These rocks represent primarily rain-out of glacial debris and form poorly to well defined bedding planes.
Conglomerate Facies	Poorly sorted conglomeritic beds which represent water re-working of unlithified diamacite, and high density gravity flows.
Mudrock with stone Facies	This facies consists of well laminated shale or rythmite deformed by clasts, these deposits were formed by rain-out.
Mudrock Facies	Deposited through suspension settling or sediment fall-out from underflows loaded with silt. The facies is usually dark in colour and commonly carbonaceous mudstone, shale or silt.
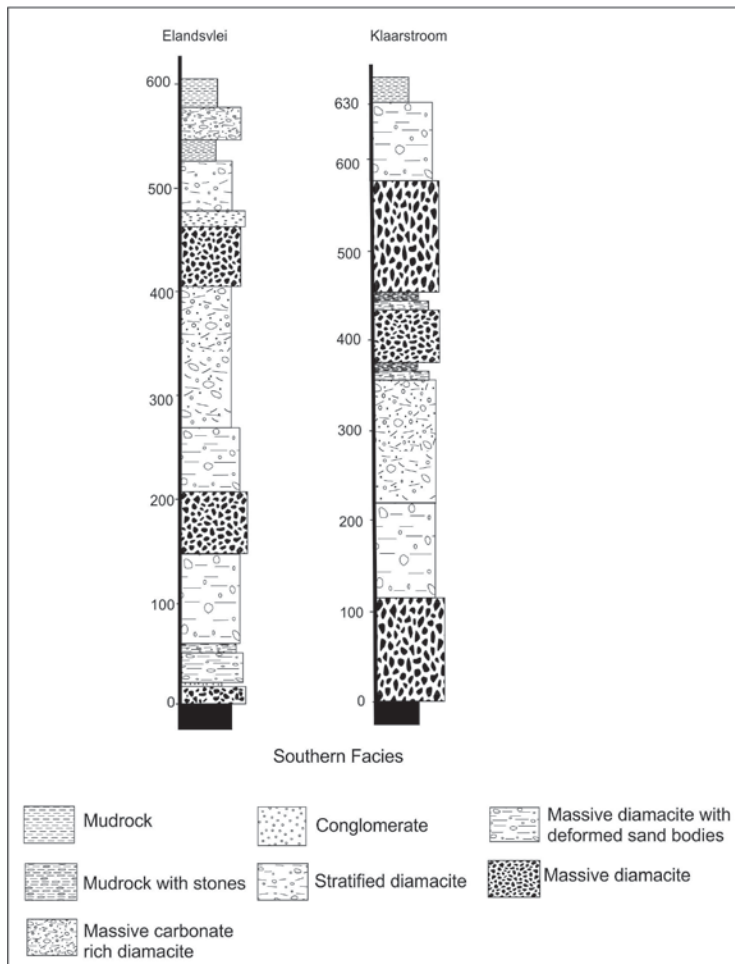
Figure 12: Profile of the lithological facies of the Elandsvlei Formation or Southern Facies (Johnson *et al*., 2006)

3.2 Geomorphology

Figure 13 shows the prevalence of the African Erosion Surface in the Grahamstown region upon which the pan(s) in this study are located. The Grahamstown silcrete is present at or close to the African Erosion Surface in most places.
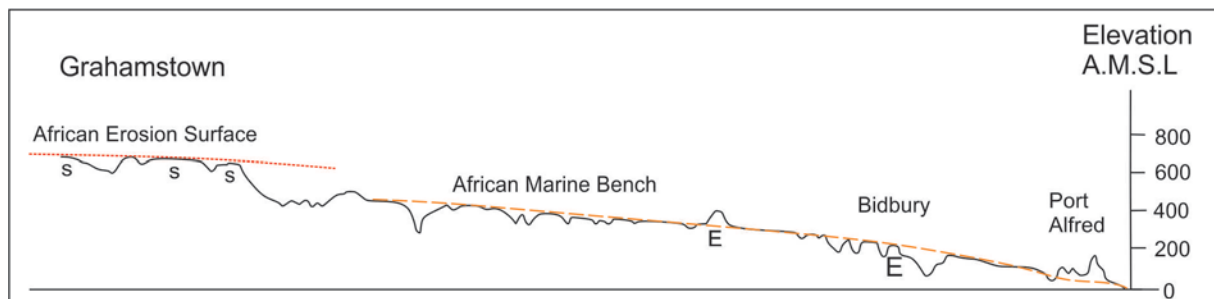
Figure 13: Cross sections of the hinterland in the Grahamstown region showing the African Erosion Surface and other prevalent erosion surfaces (adapted from Maud, 1996). S = silcrete, E = Eocene marine sediments

3.3 Climate

Grahamstown falls in the intersection of four climatic zones: two temperate coastal zones from the west and the east, and two zones in the interior which are hot and dry (Steynor, 2006). It is the intersection of these zones that is largely responsible for the variable climate experienced in Grahamstown. Grahamstown has an average rainfall of 550-600 mm annually, and a potential evaportranspiration rate of 1000-1500 (Shackleton *et al.,* 2007; Vogel, 2000).

3.4 Vegetation

Grahamstown is situated within close proximity of four biomes, the Grassland biome to the north-east, the Cape Fynbos to the west, the Karoo to the north-west, and the Albany Thicket that occupies most valleys (Shackleton *et al.,* 2007). The most prominent biome around Grahamstown is the Albany Thicket, which is the second smallest biome in South Africa and takes up 3.3 % of the total land area (Pote *et al.,* 2006). It is a mix of arid and semi-arid, and succulent vegetation, which typically grows in extensive thickets (Pote *et al.,* 2006).

3.5 Land Use

A number of pans on the African Erosion Surface occur on the Grahamstown Commonage, which falls under the jurisdiction of the Parks and Reaction Division of Makana Municipality (Davenport *et al.*, 2012). The commonage is used primarily for recreation and for subsistence livestock production, including cattle, sheep and goat farming (Shackleton *et al.,* 2007). The commonages around Grahamstown can be separated into three sections. The Southern Commonage, which is now part of the Oldenburgia Conservancy, occurs to the south-west of the city, the New Commonage to the north, made up of a group of small holdings that serve to help emerging farmers in the area, and the Eastern Old Commonage, which is used for subsistence farming (Davenport and Gambiza, 2009). The study area is located in the New Commonage.

Grahamstown has experienced rapid population growth over the last decade, due to an influx of migrants from rural areas. The population is estimated to have increased from 82, 682 in 2001 to over 100 000 presently (Davenport *et al.,* 2012).

3.6 Study Location

The primary study area (pan A) is situated on the Municipal Commonage outside of Grahamstown, north-east of the Grahamstown Military Base (Figure 14). The pan lies on a silcrete plateaux at 665 metres above sea-level, and is located at 33° 16.107 S and 26° 30.975 E. Natural Albany Thicket surrounds the pan entirely, and the pan is spatially removed from any roads and housing. The pan is inundated for most of the year and dry over the late summer months. The pan presents an ideal location for the study, as it is in a relatively pristine condition, eliminating any cause and effect considerations of human interaction. The commonage is free of signs of overgrazing though small buck and cattle do occur in the area.
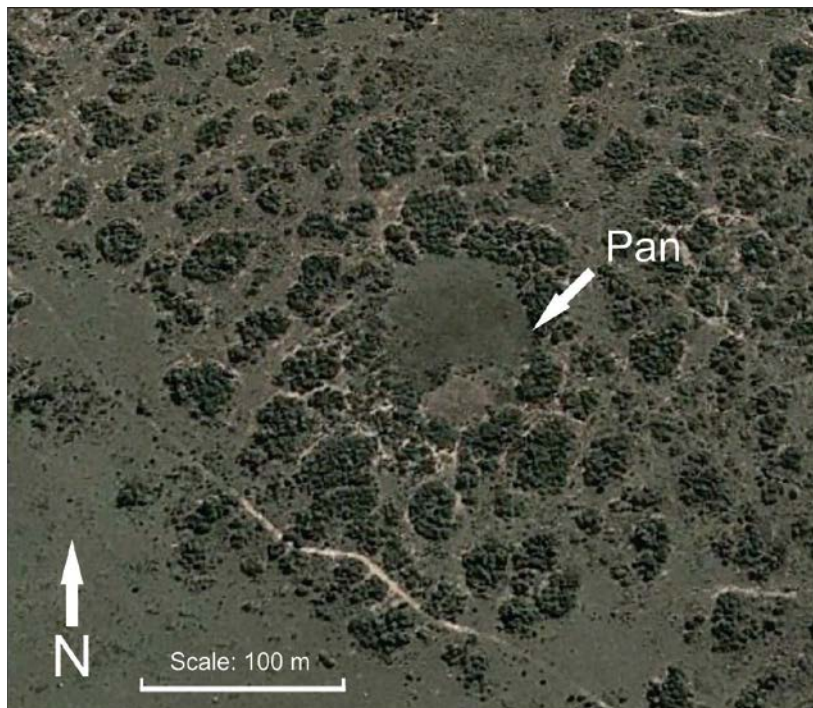
Figure 14: Aerial view of the pan

Chapter 4: Methods

4.1 Assessing surface-groundwater interactions

A total of 6 slotted PVC piezometers were placed around Pan A in core holes drilled manually by auger to depths of up to 2.3 m. The piezometers contained 3 cm long slots positioned every 25 cm on alternating sides along the length of the piezometer. The peizometers were placed in two perpendicular transects that extended through a common point in the centre of the pan. Each piezometer was placed at varying distance outward from the water mark at the time of sampling following prolonged heavy rains, the first being approximately 5 m from the water's edge and thereafter they were placed 10 m apart. Water elevation in the pans was measured relative to a fixed peg and water samples were collected from the pans over time to measure electrical conductivity, total dissolved oxygen, total dissolved solids and pH.

4.2 Sampling of weathered material

A total of 8 cores were excavated at Pan A by auguring, of which 6 were used to measure groundwater depth in the slotted peizometers described above. A further 2 cores were excavated, one at the centre of the pan and another 5 m from the water's edge east of the pan. Cores were described based on their degree of mottling, colour variations, gross grain size distribution and cohesive properties. Samples were collected where there were observable significant changes in one or more of these properties with depth, or where no changes were observed at depth intervals of 0.5 m. Sample depth was limited by the difficulty of collecting deep samples, such that less weathered material could not be sampled. The cores were positioned to provide insight into variation in soil characteristics from the centre outwards beyond the edge of the pan.

4.3 Topographic Surveying

The topography of the pan and the surrounding area was determined by dumpy level surveying. Numerous cross-sections of the pan were surveyed including the positions and elevations of all cores and piezometers. In order to add context to the topography of the pan, surrounding areas were also surveyed to allow the pan to be understood in relation to the adjacent land surface. The

elevation of the pan above mean sea level was determined by surveying to the nearest trigonometric beacon.

4.4   Sample Preparation and Crushing

The core samples were dried in an oven for two days at 50 °C. Samples for XRF and XRD analysis were crushed in a manganese-alloy swing mill for six minutes each. Due to the high clay content of the samples, fine crushing was then carried out in an automatic mortar and pestle, and where necessary, samples were further crushed manually in a mortar and pestle. In some cases samples were placed in the swing mill for a further 15 minutes to produce fine enough samples for chemical analysis.

The sample of tillite was crushed using a jaw-crusher and milled in a tungsten carbide vessel at the XRD and XRF Facility at the University of Pretoria.

4.6   X-Ray Fluorescence

Bulk rock analysis of trace and major elements was completed using XRF analysis. Samples were prepared for XRF analysis using the method of Norrish and Hutton (1969). Powder pellets were made using 5 g of fine grained powder poured into an aluminum sleeve and gently pressed with a perspex rod into a cake. The aluminum sleeve and perspex rod were then carefully removed from the barrel. Excess powder was removed from around the surface of the pellet and the barrel replaced. Boric acid was then poured down the barrel and a steel plunger was placed in it. The plunger assembly was then subjected to a pressure in excess of 10 tons. The Pellet was then freed from the barrel by inverting the plunger assembly, covering it with a perspex cover, and exerting hydraulic pressure until the pellet was released from the barrel. The mortar and pestle, plunger assembly, aluminum sleeve and perspex rod were cleaned with distilled water and wiped with acetone before making a new pellet.

The preparation of fusion disks began with the cleaning silica crucibles with distilled water and drying them in an oven at 120 °C for 30 min. The crucibles were left to cool in a desiccator. Once cool, crucibles were weighed on a high precision balance and 2 g of rock powder was measured in each one. To determine the surface moisture content (H_2O) of each sample, the

crucibles containing rock powder were placed in an oven at 110 °C for three hours, after which time the crucibles were removed and again placed in a desiccator to cool. Once cooled, the crucibles were reweighed and the loss of weight was expressed as a percentage of the original powder weight. The crucibles were then placed in a furnace at 1000 °C for approximately 10 hours, after which time they were removed and placed in desiccators to cool. The crucibles were then reweighed and the Loss On Ignition (LOI) was expressed as a percentage of original powder weight. The powder was then transferred from the crucibles into labeled glass vials. The fusion mixture was prepared by recording weights of approximately: 1.5000 g of flux, 0.2800 g of powder, and 0.0200 g of $NaNO_3$. Prior to the preparation of the fusion mixture, the flux was heated in a furnace at 450 °C for a minimum of three hours and the $NaNO_3$ was heated in an oven at 120 °C. Both the flux and the $NaNO_3$ were cooled in a desiccator post heating. The flux and $NaNO_3$ fusion mixture was then placed in labeled glass vials sealed with mylar film, and stored in a desiccator. When manufacturing the fusion disks, the fusion mixtures were thoroughly mixed. Hotplates were allowed to heat, after which the gas burner was lit. The fusion mixture was then poured into a platinum crucible and, handling the crucible with platinum tipped tongs, it was placed over the gas burner and left until the fusion mixture had melted to the point of complete homogenization. The bead of melt was then tipped onto a granite mould and pressed. The resulting glass disk was tipped onto an asbestos pad on the hotplate so that it could slowly cool. The platinum crucible was then dropped into distilled water in order to quench any leftover beads of melt, which were then removed from the crucible before continuing to the next sample.

The sample of tillite collected from near to the pan was obtained from a core sample that had been drilled for the purposes of groundwater exploration. This sample was processed by the University of Pretoria XRF analysis lab. The sample was crushed in a tungsten-carbide milling pot, then dried at 100 °C and placed into a furnace at 1000 °C to determine LOI. A 1g sample was mixed with 6g of Lithium-teraborate flux and fused at 1050°C to make a stable fused glass bead for major element chemical analysis. For trace element analysis the sample was mixed with a PVA binder and pressed into a pellet using a 10 ton press. The Thermo Fisher ARL9400 XP+ Sequential XRF with WinXRF software was used for analysis.

4.7   X-Ray Diffraction

X-Ray powder diffraction analysis was carried out using a Discover D8 Bruker XRD Diffractometer System. Sample data were sent to the XRD and XRF Facility at the University of Pretoria where qualitative and quantitative analysis was carried out. The phases present in the samples were identified using X'Pert Highscore Plus software, and the relative phase amounts in weight % were estimated using the Rietveld method (Autoquan Program). Errors were given on the three sigma level.

A second sample of tillite sourced from the study area was also sent for full XRD analysis. The sample was analysed using a PANalytical X'Pert Pro powder diffractometer with X'Celerator detector and variable divergence and receiving slits with Fe filtered Co-Kα radiation. This sample was also qualitatively and quantitatively analysed in the same manner as the other samples.

4.8   Volume loss calculations to determine pan origin

Volume change was calculated using Equation 11 as described by White *et al*. (1996).

Equation 11: Volume Change Calculation (White *et al*., 1996)

$$V_p = \left(\frac{\rho_p}{\rho_w}\right) \times \left(\frac{C_{i,p}}{C_{i,w}}\right) - 1$$

where *Vp* is the volume change.

The term ρ_p is the density of the parent material and ρ_w is the density of the weathered material. The term $C_{i,p}$ is the concentration of an immobile element in the parent material, while $C_{i,w}$ is the concentration of an immobile element in the weathered material.

The $\left(\frac{C_{i,p}}{C_{i,w}}\right)$ component of the equation is included to account for relative changes in elements and minerals which could affect the volume calculations. The immobile element used in this study is Zr, which was chosen based on the element mobility results.

Densities for parent materials were calculated by multiplying mineral densities by their weight percentage of the relevant sample. The density of minerals was sourced online from the

Mineralogical Database Webmineral (2012) and relevant information is shown in Table 6. Where *Vp* is zero, there has been no volume change, where it is positive it indicates volume expansion, and where it is negative it indicates volume reduction (White *et al*., 1996).

Table 6: List of relevant minerals and their densities (Mineralogical Database Webmineral, 2012)

Minerals	Density
quartz	2.62
plagioclase	2.68
Kaolinite	2.6
Calcite	2.71
Chlorite	2.65
Zircon	4.65
Dolomite	2.84
Magnetite	5.15
Muscovite	2.82
Goethite_	3.8
Hematite	5.3
Rutile_	4.25
Anatase	3.9
Microcline	2.56

Volume changes per core were calculated up to depths of 130-160 cm for easy comparison across cores A1-A6 and the centre core AC. Individual volume losses and volume gains calculated for samples in a core were added to determine the overall volume change for that core, as shown below (Table 7), for example, in core A1.

Table 7: Example of volume change calculations per core using data from core A1

Sample	Vp
A1 0-10	-0.631
A1 70-75	0.154
A1 100-110	-0.127
A1 150-160	-0.131
Sum (Vp for core)	**-0.735**

Chapter 5: Results

5.1   General description

The pan occurred within a closed contour (660 m amsl) near the crest of a gently sloping land surface, with a valley sloping away from the crest of the hill towards the north (Figure 15). The distribution of vegetation is not related to the topography in any way, comprising dense thicket and grassland vegetation, which are dominated by woody plants less than 5 m high and grasses respectively. The pan is dominated by herbaceous wetland plants and is surrounded by thicket.
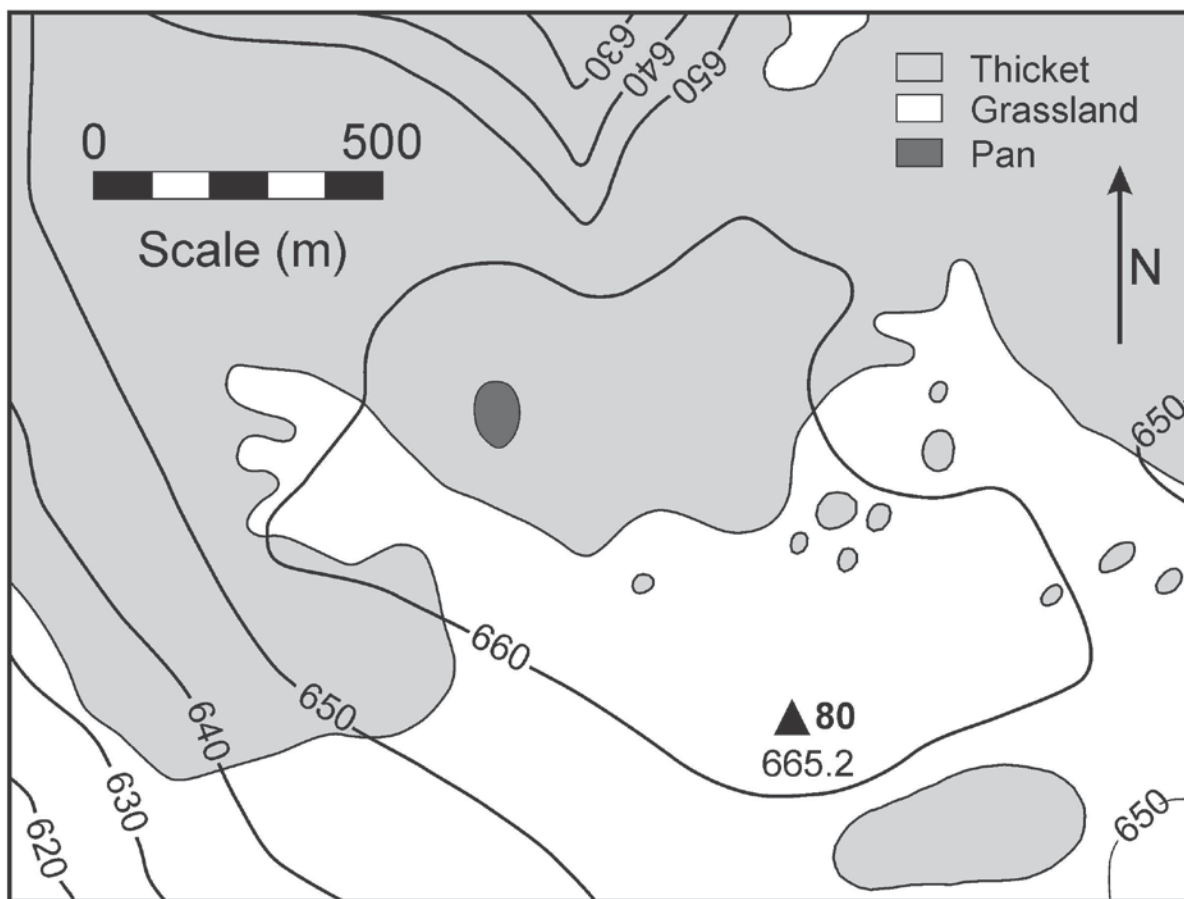
Figure 15: Contour map of the area of Pan A showing vegetation types, the location of the pan and Trig Beacon 80 at an altitude of 665.2 m amsl.

Pan A covered a total surface area of approximately 16 775 m^2 (1.68 ha) and was kidney shaped (Figure 16) with two distinct depressions in the pan; the larger one was termed the primary pan as it was the deepest and most central. In contrast, the secondary pan was approximately 40 cm shallower at its greatest depth and was situated north of the primary pan. Reference from here on refers to the primary and secondary pan together, which form the greater pan system. The northern and north-western slopes into the pan were more gentle than the slopes on the southern and eastern sides, and the soil along the northern and north-western sides of the pan was more saturated than that along the southern and eastern sides. The southern end of the pan is also more vegetated with thicket starting beyond A1 and A4, and steadily thickening outward.

Transect A-B shows the profile across the longest axis of the pan and the relative positions and elevations of the primary and secondary pans, while transect C-D was across the short axis of the pan (Figure 17a and 17b). The local relief is extremely low (slightly more than 1 m change in elevation across the pan), and slopes are very gentle at generally less than 2.5 %. Figure 18 is a transect from the benchmark of the pan to trig beacon MO-IE-80, showing that the pan was located in an extremely flat locale. The altitude changed approximately 4 metres (m) over a distance of 636 metres (m), representing an average gradient of 0.6 %.

Figure 16: Morphology of the pan showing contour lines, water's edge at the time of the survey, positions of cores and the permanent bench mark.
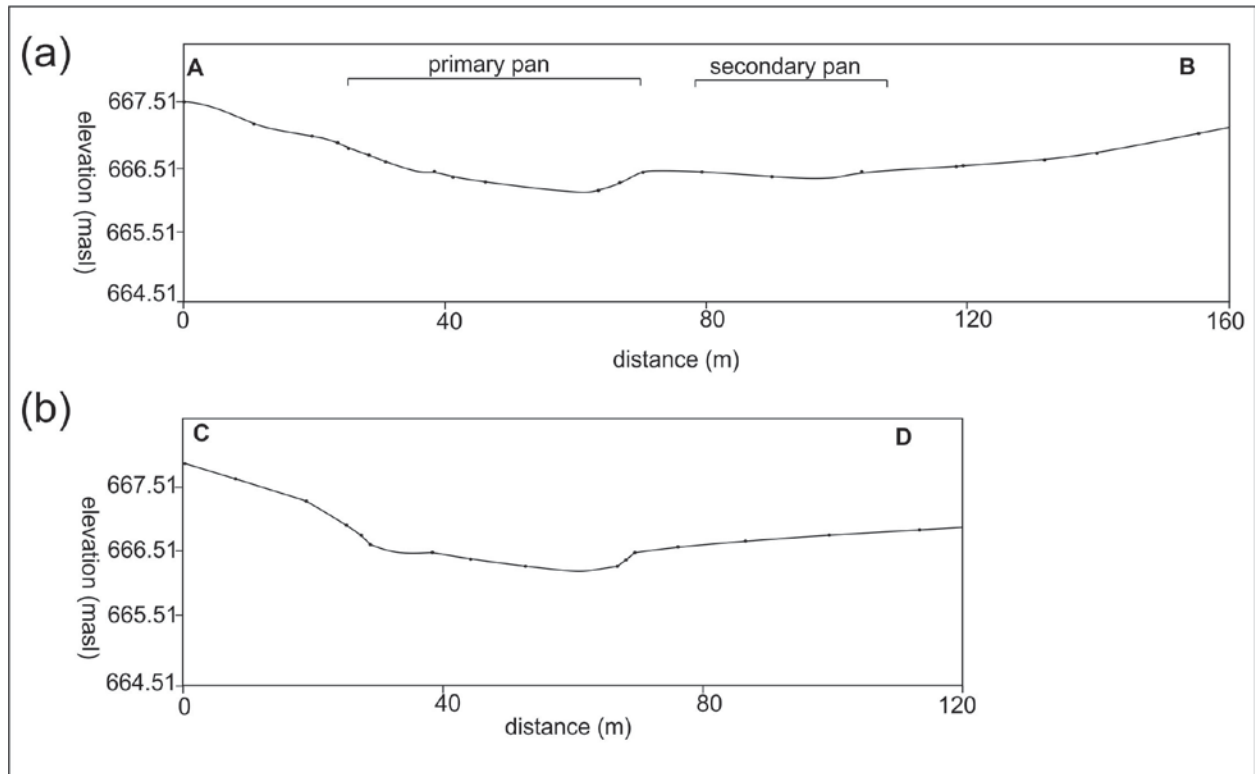
Figure 17: Topographic profiles along transects (a) A-B, showing the position of the primary and secondary pan along the long axis of the pan, and (b) C-D showing the short axis across the pan.
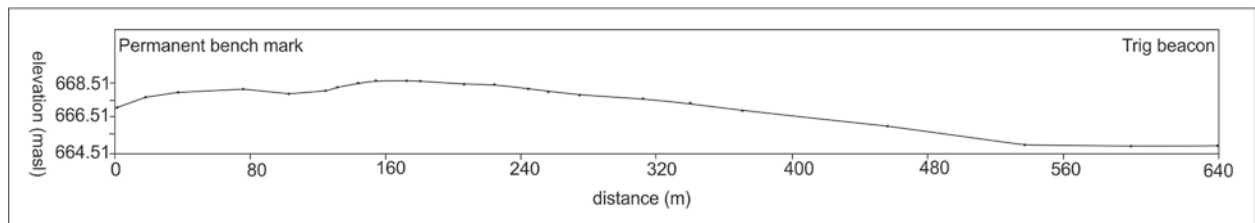
Figure 18: Topographic profile of the area surrounding the pan from the permanent bench mark of the pan to the trig beacon.

5.1   Water Table interaction

In Pan A, six piezometers were placed in cores A1, A2, A3, A4, A5 and A6 (Figure 16). The water table was not encountered in any of the piezometers except the one at the centre of the pan (AC), remaining dry throughout the four month long wet season over which the water table was monitored. Following the monitoring period, the water level in Pan A decreased to a point where the pans dried up completely. Water electrical conductivity (EC) and salinity in Pan A increased

over the months from August to October by approximately a factor of 2 (Table 8). The pH of the water in the pan was high with

values of approximately 9. From January the pan was dry.

Table 8: EC data collected from Pan A during monitoring over August to January (when the pan was dry).

Date	EC1	EC2	Sal	DO %	pH
17/08/2011	127	103	0.81	0.7	8.88
22/09/2011	192	172	0.09	1.7	9.06
18/10/2011	262	232	0.12	5.2	9.6

5.2   Descriptions of cores

Descriptions of soil cores are presented for Cores A1, A2 and A3 on the south-eastern steep slope into the pan. Material at the surface was generally dark brown close to the pan and became lighter coloured further from the pan (Figure 19). Surface sediment was generally sandy and there was commonly an increase in the fine fraction (silt + clay) with depth. Silcrete nodules were present at or close to the soil surface, with the size of these nodules increasing progressively further away from the pan as well as at depth in all cores, from a depth of 1m in the case of the core closest to the pan, about 2 m in Core A2, and occasionally in Core A3. Mottling, albeit generally very indistinct, was present at variable depths, from approximately 0.7 m in the core closest to the pan, and at shallower depths in Core A2. Mottling was largely absent from the core furthest away from the pan and was most clearly evident in the core closest to the pan (Core A1). Calcium carbonate aggregates were present in association with silcrete nodules at a depth greater than 1.2 m in the case of Core A1, at a depth greater than 1.3 m in the case of Core A2, and between a depth of 1 and 1.5 m in the case of Core A3. Soils became increasingly brightly coloured ("orange-red") at a depth of 1.2 m in Core A1 and 1.5 m in the case of Core A2. Soil core A3 at these depths could be described as "orange-brown". A striking feature of Core A3 was the presence of kaolinite that appeared as off-white aggregates at a depth of 1.2 m, with the abundance of kaolin increasing with depth and becoming increasingly white .
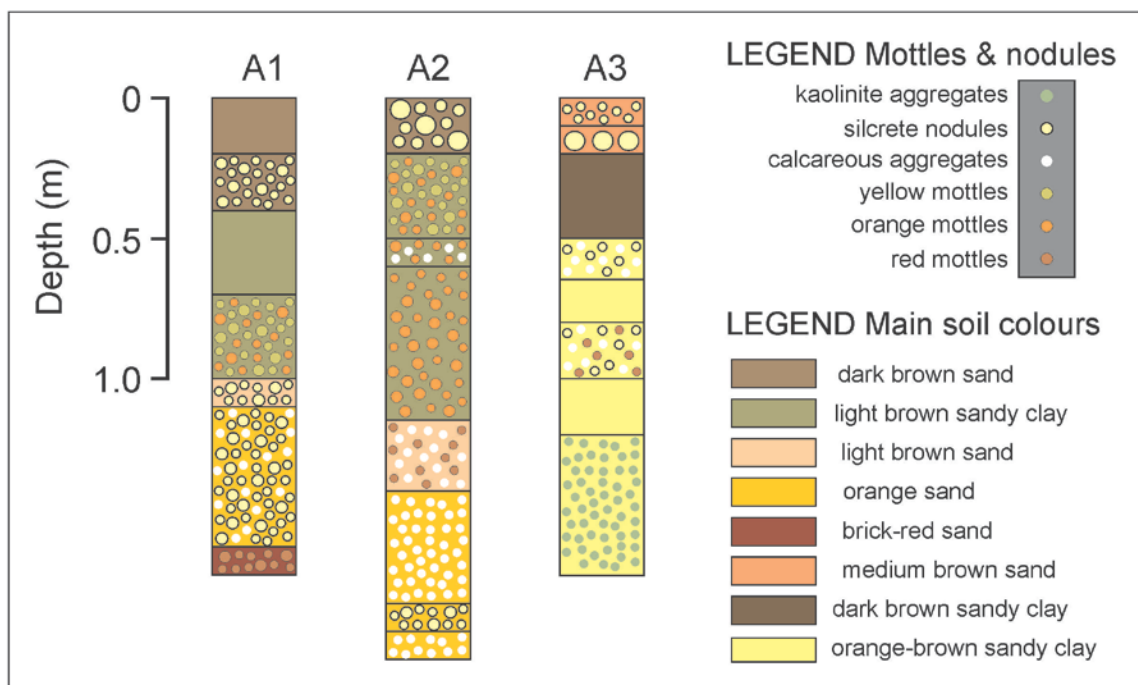
Figure 19: Schematic depiction of cores as described in the field.

5.3 Geochemical analysis from XRF analysis

5.3.1 Geochemical relationships in relation to elements typically conserved during weathering

Results show substantial variation in element concentration with depth and with respect to the proximity of the core to the centre of the pan (Table 9). The overall concentration of SiO_2 was highest, followed by Al_2O_3, Fe_2O_3 and CaO.

In general, cores A1, A2, A3, A4, A5 and A7, which all lie outside of the inundated area of the pan, had very high SiO_2 concentrations close to the surface (mean = 68.2 %; standard deviation = 5.22 %) that declined sharply below the surface (mean = 49.9 %; standard deviation = 10.66 %). For the sample in the centre of the pan (core AC), SiO_2 declined far less markedly from the surface (59.9 %) with increasing depth (mean = 55.1 %; standard deviation = 2.45 %).

The concentration of Al_2O_3 showed the opposite trend for the same samples, with a marked increase in concentration below the soil surface of cores at the highest elevations and at greatest and intermediate distances from the pan (cores A1, A2, A3, A4, A5 and A7). Surface samples

had a mean concentration of 8.32 % (standard deviation = 0.79 %), while subsurface samples had a mean concentration of 14.41 % (standard deviation = 2.44 %).

Table 9: Geochemical composition of samples from XRF analysis in weight percent (wt %). Zr (ppm) is added in the last column.

Core	Depth (cm)	SiO_2	TiO_2	Al_2O_3	Fe_2O_3	MnO	MgO	CaO	Na_2O	K_2O	P_2O5	LOI	H_2O	TOTAL	Zr (ppm)
A1	0-10	73.6	0.61	7.4	8.0	0.06	0.37	0.33	0.80	0.94	0.07	5.5	1.60	**99.2**	514.3
	70-75	46.7	0.62	14.6	11.1	0.05	1.58	4.63	0.33	1.19	0.12	13.5	4.54	**98.9**	173.1
	100-110	47.9	0.65	14.6	4.9	0.05	4.07	6.65	0.27	0.96	0.08	15.2	4.60	**100.0**	219.4
	150-160	49.1	0.65	15.3	8.4	0.06	1.74	5.40	0.33	1.23	0.07	13.3	3.92	**99.5**	219.1
A2	0-10	69.7	0.64	8.9	8.4	0.05	0.35	0.36	0.65	1.04	0.09	6.8	2.42	**99.4**	498.6
	60-70	44.2	0.65	15.6	15.3	0.05	1.12	2.74	0.13	1.08	0.09	11.6	5.81	**98.4**	168
	120-130	36.5	0.64	11.3	6.2	0.03	4.50	13.87	0.12	0.83	0.06	21.9	3.43	**99.3**	165.1
	180-190	41.4	0.63	13.5	11.6	0.02	3.84	7.09	0.15	0.79	0.08	16.9	3.85	**99.8**	175.1
A3	0-10	65.1	0.66	9.2	11.9	0.06	0.37	0.40	0.55	0.95	0.10	8.0	2.28	**99.4**	409
	60-70	42.7	0.54	16.9	6.5	0.05	1.57	7.34	0.14	1.49	0.07	16.3	5.03	**98.6**	166.2
	80-90	26.0	0.34	10.4	3.6	0.04	1.75	24.48	0.09	1.03	0.09	26.9	3.45	**98.2**	77.4
	130-140	35.0	0.48	11.9	4.2	0.04	3.96	15.90	0.11	1.02	0.07	22.0	4.52	**99.2**	127.7
A4	0-10	65.0	0.66	7.3	16.0	0.04	0.29	0.22	0.58	0.84	0.13	6.2	2.22	**99.5**	316.7
	60-70	66.2	0.51	9.4	6.0	0.02	0.85	3.31	0.76	1.29	0.06	7.3	3.75	**99.5**	367.6
	120-130	64.5	0.63	13.3	6.4	0.02	1.10	0.45	0.69	1.67	0.05	5.4	5.57	**99.8**	291.9
	160-170	56.5	0.87	16.4	6.1	0.03	1.86	1.93	0.32	0.98	0.09	10.8	3.11	**99.0**	243
A5	0-10	74.3	0.64	8.6	4.9	0.09	0.40	0.42	0.94	1.16	0.07	6.0	2.02	**99.5**	545.8
	50-60	51.6	0.66	16.3	10.7	0.04	1.46	0.76	0.53	1.75	0.08	8.8	6.57	**99.2**	181.6
	120-130	62.2	0.95	17.6	4.4	0.03	0.77	0.28	0.28	0.55	0.07	8.3	3.63	**99.1**	303.1
	150-160	52.0	0.79	17.6	11.8	0.05	1.02	0.49	0.37	1.03	0.11	10.1	3.66	**99.0**	185.9
	185-190	57.6	0.91	17.0	6.3	0.05	1.01	2.00	0.35	0.94	0.10	10.3	3.10	**99.6**	254.9
	210-220	61.7	1.00	14.7	10.0	0.04	0.57	0.34	0.26	0.67	0.12	7.1	3.37	**99.9**	285.4
A6	0-10	52.5	0.64	15.8	10.6	0.02	0.76	0.30	0.79	1.45	0.07	11.3	4.97	**99.2**	474.1
	60-70	53.4	0.59	15.6	7.8	0.07	1.46	1.82	0.41	1.59	0.06	11.0	4.86	**98.7**	251
	80-90	46.1	0.54	14.3	6.4	0.05	1.70	8.26	0.38	1.42	0.08	13.6	6.23	**99.0**	180.5
	140-145	56.1	0.84	14.7	11.4	0.06	1.10	0.67	0.36	0.90	0.11	9.2	3.71	**99.2**	257
A7	0-10	61.3	0.70	8.5	16.8	0.05	0.35	0.27	0.53	0.81	0.13	7.8	2.36	**99.5**	265.8
	60-70	53.3	0.74	16.2	9.2	0.06	1.49	0.42	0.24	1.20	0.05	10.6	5.27	**98.8**	160.7
	70-80	53.1	0.92	13.1	15.1	0.05	1.03	0.32	0.21	0.92	0.08	9.0	5.09	**98.8**	185.3
AC	40-50	59.9	0.64	13.4	7.1	0.04	1.06	0.66	0.61	1.80	0.05	9.3	4.33	**98.9**	231.5
	50-60	55.8	0.64	14.4	7.7	0.04	1.30	3.06	0.53	1.91	0.06	8.7	6.07	**100.2**	174.1
	90-100	53.5	0.70	16.9	8.4	0.03	1.31	1.23	0.46	1.92	0.06	8.7	6.33	**99.5**	163.2
	110-120	54.6	0.86	20.2	7.0	0.03	1.20	0.42	0.33	1.37	0.06	10.0	3.68	**99.7**	224.9
	130-140	52.6	0.77	18.5	5.2	0.02	1.20	4.47	0.29	1.22	0.06	11.0	4.63	**100.0**	198.3
	140-145	58.9	0.68	17.8	6.0	0.04	0.91	1.55	0.26	0.95	0.06	8.7	3.91	**99.8**	202.1
Mean		**54.3**	**0.69**	**13.9**	**8.6**	**0.04**	**1.41**	**3.51**	**0.40**	**1.17**	**0.08**	**11.1**	**4.11**	**99.3**	**253.1**

For cores A1, A2, A3, A4, A5 and A7, the concentrations of MgO and CaO were low at the soil surface with mean concentrations of 0.36% and 0.33% respectively (standard deviations were 0.04% and 0.08%). Concentrations of these elements typically increased with depth up to 1.5 m, below which concentration generally decreased. In the case of MgO, maximum concentrations in cores A1, A2 and A3 were reached at depths of between 1 m and 1.4 m, with an average concentration of 4.18 % (standard deviation = 0.29 %). Maximum MgO concentrations in cores A4, A5 and A7 were much lower than those in A1, A2 and A3, and occurred at variable depths. For CaO, maximum concentrations in cores A1, A2 and A3 were higher than MgO, with a mean of 15.0 % (standard deviation = 8.9 %) measured at depths between 1 m and 1.3 m. In cores A4, A5 and A6 the maximum concentrations of CaO were consistently lower than for cores A1, A2 and A3 over a wide range of depths.

In all cores, Na_2O decreased relatively consistently with increasing depth, while the concentrations of K_2O showed a high degree of variability with depth. However, the lowest K_2O values were typically observed at the greatest depth within cores. The concentrations of Fe_2O_3 and MnO also varied inconsistently with increasing depth.

With the exception of surface and near-surface samples, which were enriched in SiO_2 relative to Al_2O_3 and TiO_2, there was a positive relationship between SiO_2 and $Al_2O_3,$ and SiO_2 and TiO_2 (Figure 20a and 20b). All samples showed a positive relationship between SiO_2 and Zr irrespective of depth (Figure 20c).

With the exception of samples from depth in cores A2 and A3, there was a slight increase in the concentration of MgO with increased Al_2O_3 concentration (Figure 21a). For cores A2 and A3 the increase in MgO concentration with increasing Al_2O_3 concentration was more marked. The concentration of MgO in relation to TiO_2 did not show systematic variation as TiO_2 increased, except for samples from depth in the highest-lying cores (cores A2 and A3), where there was a positive relationship between MgO and TiO_2 (Figure 21b). The relationship between MgO and Zr showed a negative relationship overall (Figure 21c).

Figure 20: Relationships between SiO2 and Al2O3 (a), TiO2 (b) and Zr (c). Blue diamonds represent subsurface samples and green triangles represent surface samples for cores on the fringe of the pan (A1 to A7), while red squares represent samples from the core in the centre of the pan (AC). Purple crosses represent a subset of the subsurface fringe samples at greatest depths in the highest-lying cores (A2 and A3).
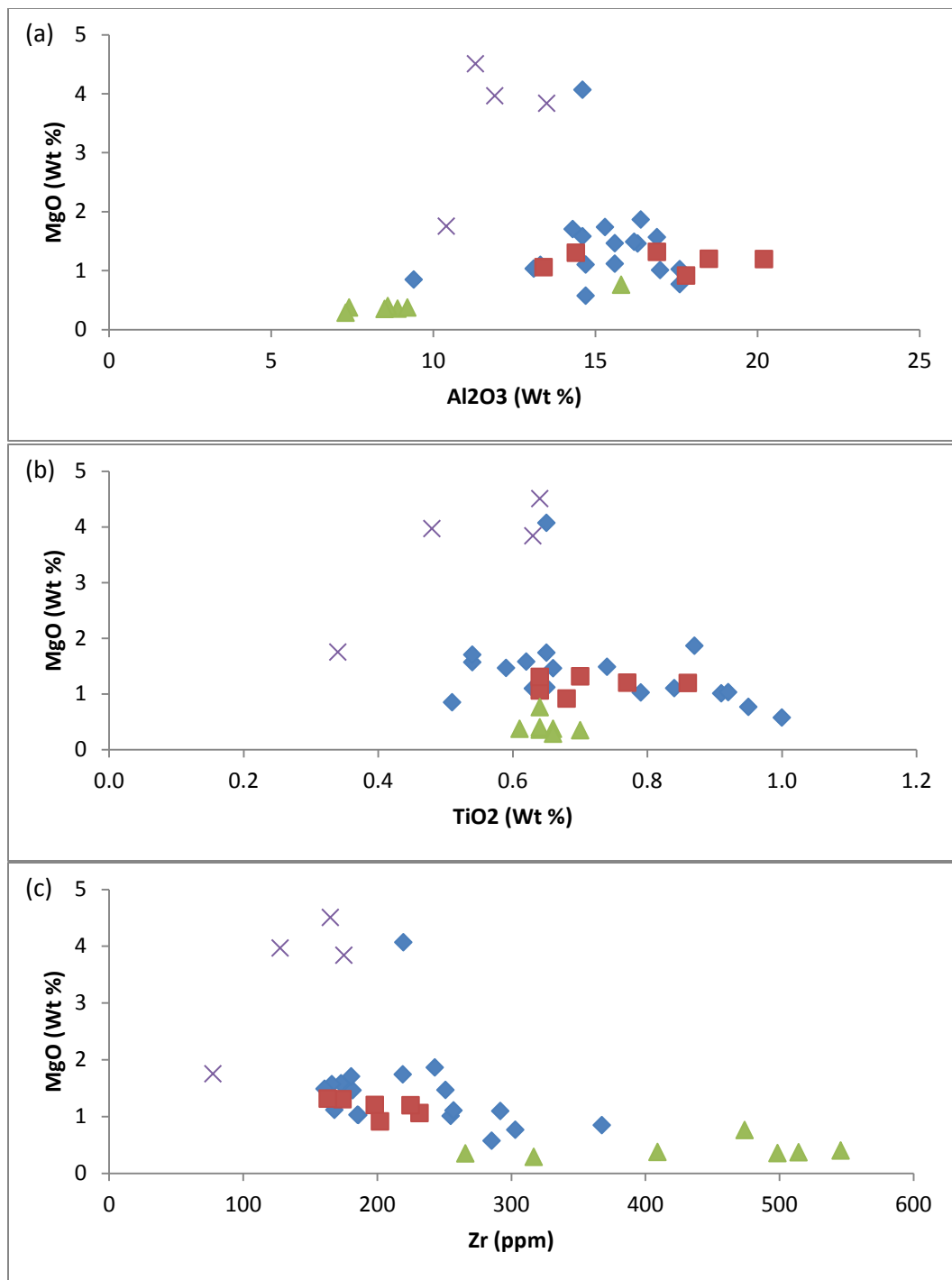
Figure 21: Relationships between MgO and Al2O3 (a), TiO2 (b) and Zr (c). Blue diamonds represent subsurface samples and green triangles represent surface samples for cores on the fringe of the pan (A1 to A7), while red squares represent samples from the core in the centre of the pan (AC). Purple crosses represent a subset of the subsurface fringe samples at greatest depth in the highest-lying cores (A2 and A3).

Generally the concentrations of CaO from samples taken at depth from the highest lying cores (A2 and A3, Figure 16) decreased with an increase in the concentration of Al_2O_3, TiO_2 and Zr (Figures 22a, 22b, 22c respectively). Relationships between CaO and Al_2O_3, TiO_2 or Zr for the remaining samples were poor.

With the exception of samples at depth from the highest-lying cores, Na_2O concentration decreased in relation to increasing Al_2O_3 and TiO_2 (Figure 23a, 23b). Excluding the core samples from the centre of the pan, the relationship between Na_2O and Zr indicated a positive trend ($R^2 = 0.76$).
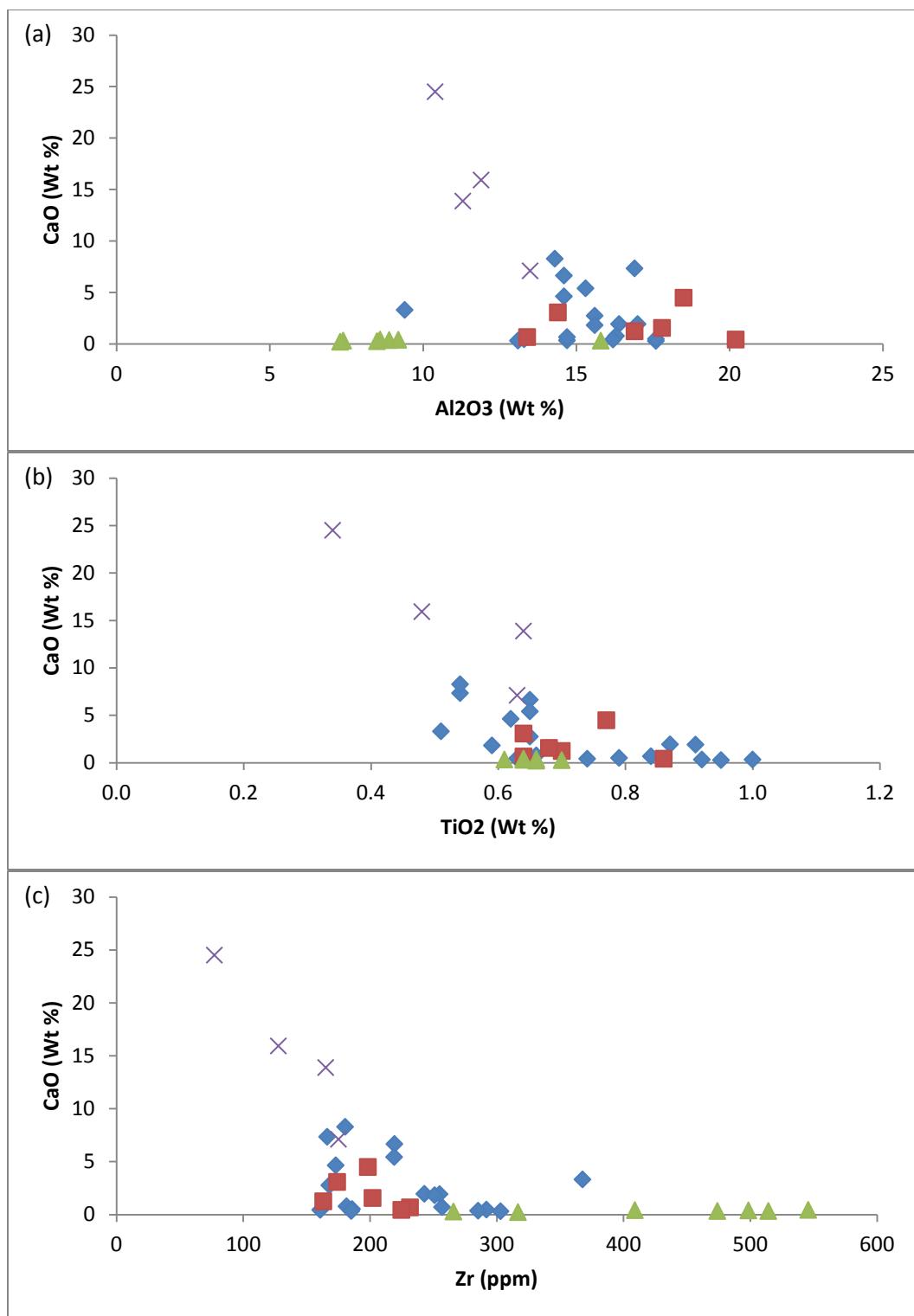
Figure 22: Relationships between CaO and Al2O3 (a), TiO2 (b) and Zr (c). Blue diamonds represent subsurface samples and green triangles represent surface samples for cores on the fringe of the pan (A1 to A7), while red squares represent samples from the core in the centre of the pan (AC). Purple crosses represent a subset of the subsurface fringe samples at greatest depths in the highest-lying cores (A2 and A3).
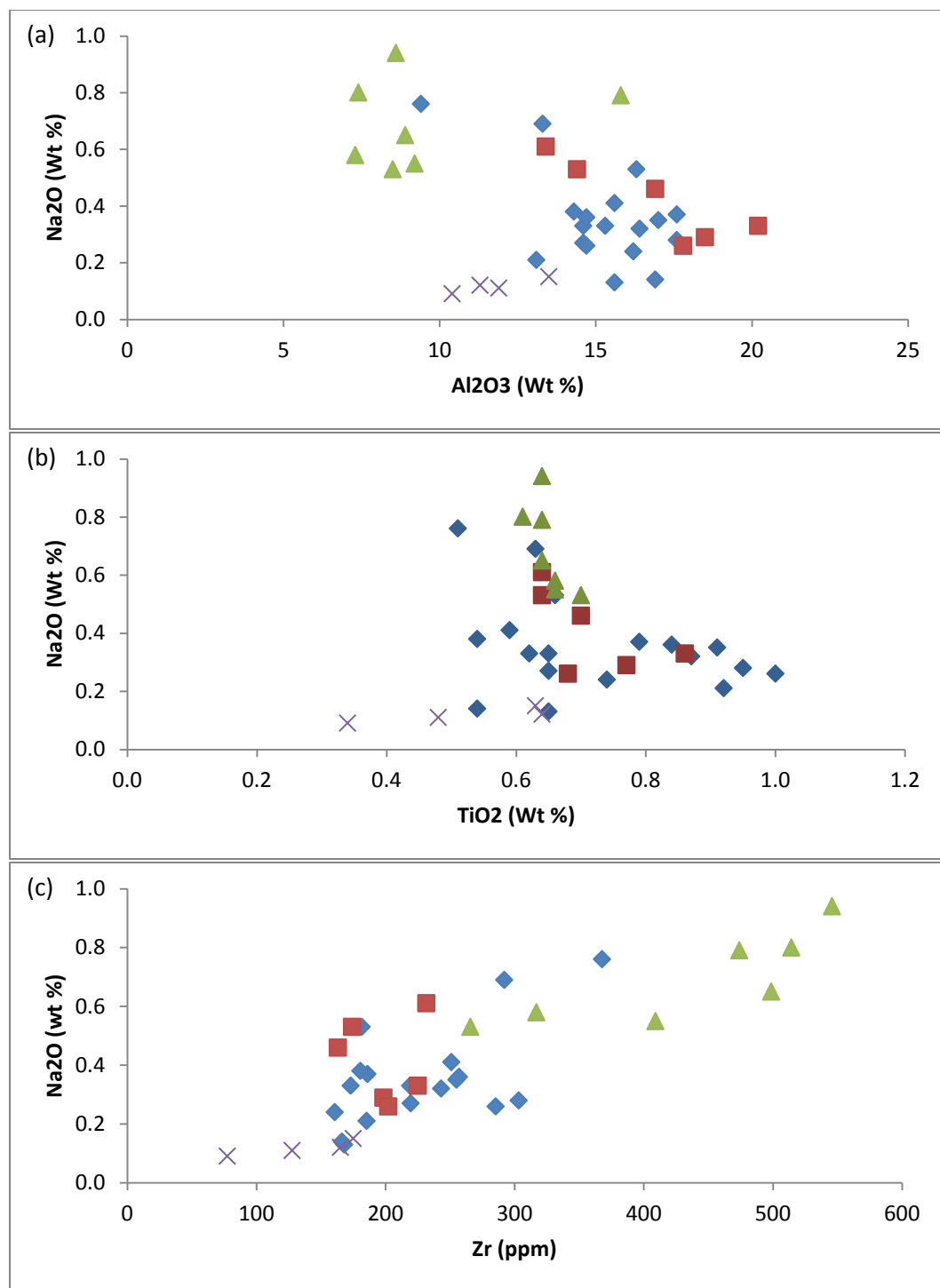
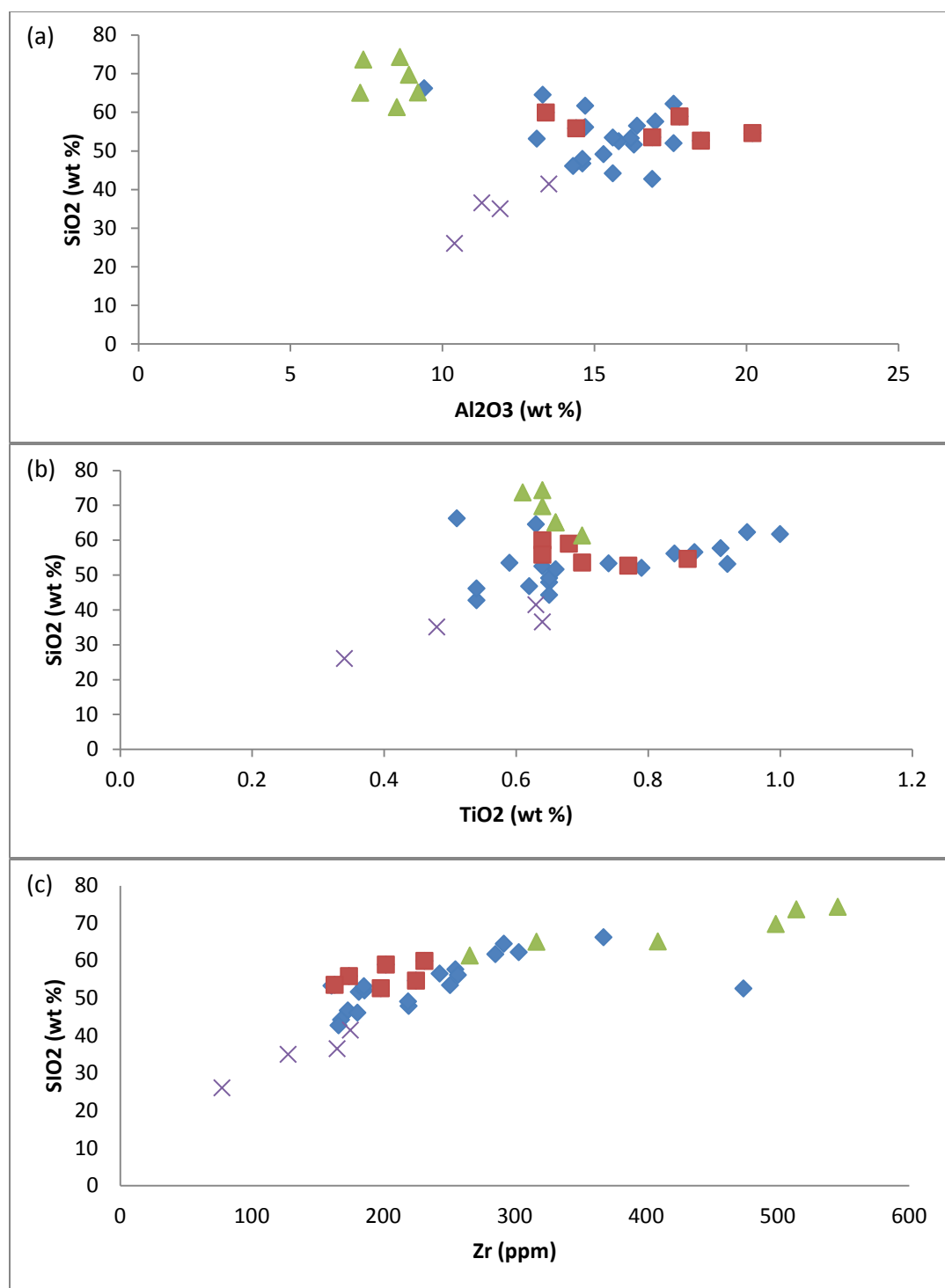**Figure 23: Relationships between Na2O and Al2O3 (a), TiO2 (b) and Zr (c). Blue diamonds represent subsurface samples and green triangles represent surface samples for the cores on the fringe of the pan (A1 to A7), while red squares represent samples from the core in the centre of the pan (AC). Purple crosses represent a subset of the subsurface fringe samples at greatest depth in the highest-lying cores (A2 and A3).**

5.3.2 Lateral and vertical geochemical relationships

The highest concentrations of silica along Transect C-E were measured at the soil surface and at depth close to the centre of the pan, with concentrations greater than 70 wt % measured at the soil surface (Figure 24a). The lowest concentrations along Transect C-E were measured at mid-depth in the core furthest from the pan's centre, where the concentration of silica was 26 wt % (Figure 24a). Concentrations along Transect F-G showed a similar decrease in SiO_2 from the soil surface to intermediate depths and an increase with depth (Figure 25a). As with Transect C-E, the concentration of SiO_2 in surface samples of Transect F-G increased from the edge towards the centre of the pan.

Isolines of Al_2O_3 concentration indicated that for both Transects C-E and F-G, the highest concentrations were at intermediate depths in individual cores, and that the overall concentration of Al_2O_3 was highest at intermediate depths in the centre of the pan (Figures 24b and 25b).

The vertical and lateral distributions of MgO and CaO in Transects C-E and F-G displayed a trend of the highest concentrations being measured at intermediate depths with increasing distance from the centre of the pan (Figures 24 (c, d) and 25 (c, d)). The CaO concentration across Transect C-E was considerably higher than across Transect F-G.

Na_2O concentrations were greatest at the soil surface and decreased with depth (Figures 24e and 25e). In the case of Transect C-E, Na_2O concentrations were highest in the centre of the pan while Transect F-G had the highest concentrations at the edge of the pan.
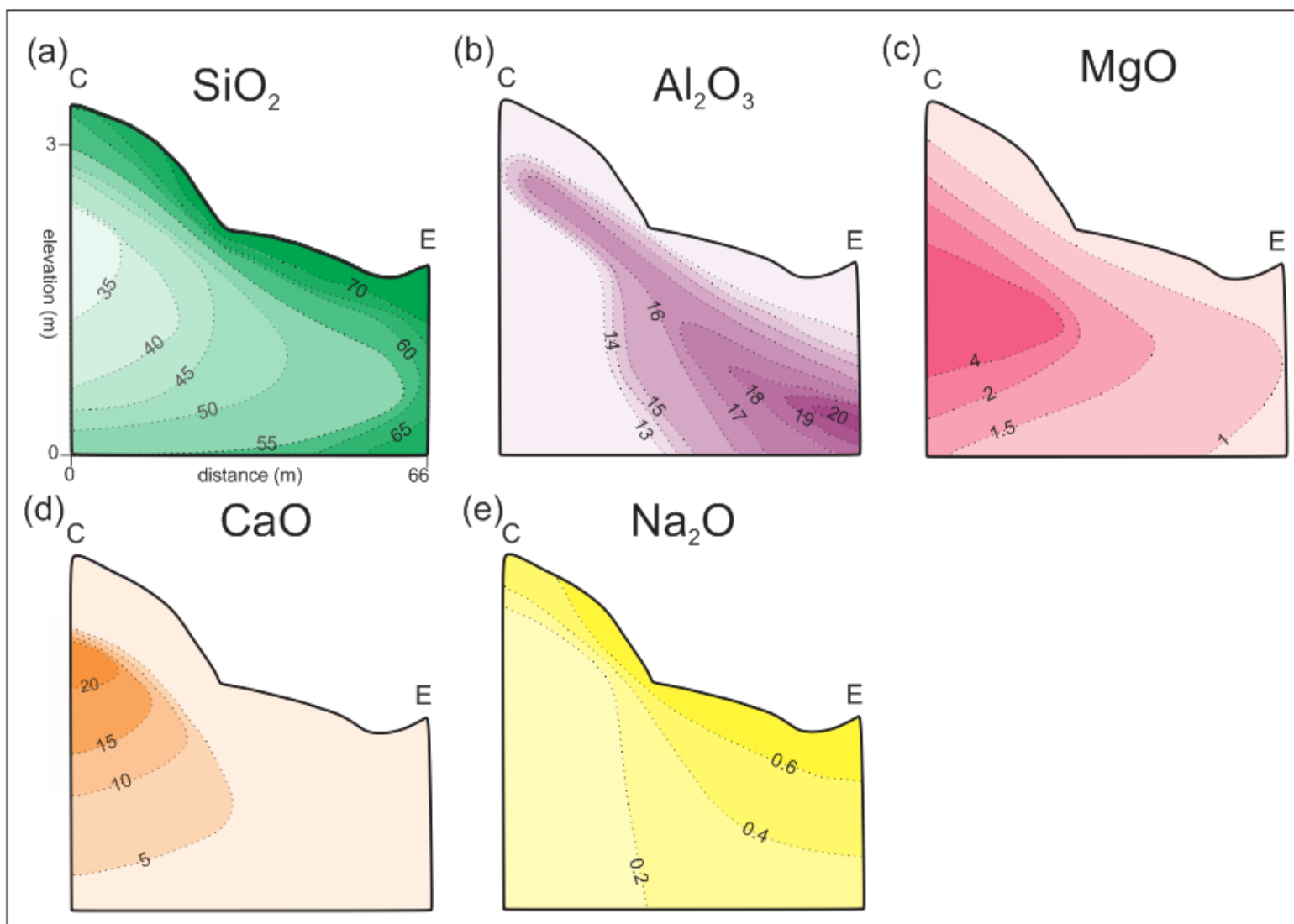
Figure 24: Subsurface geochemical isoline profiles across profile C-E
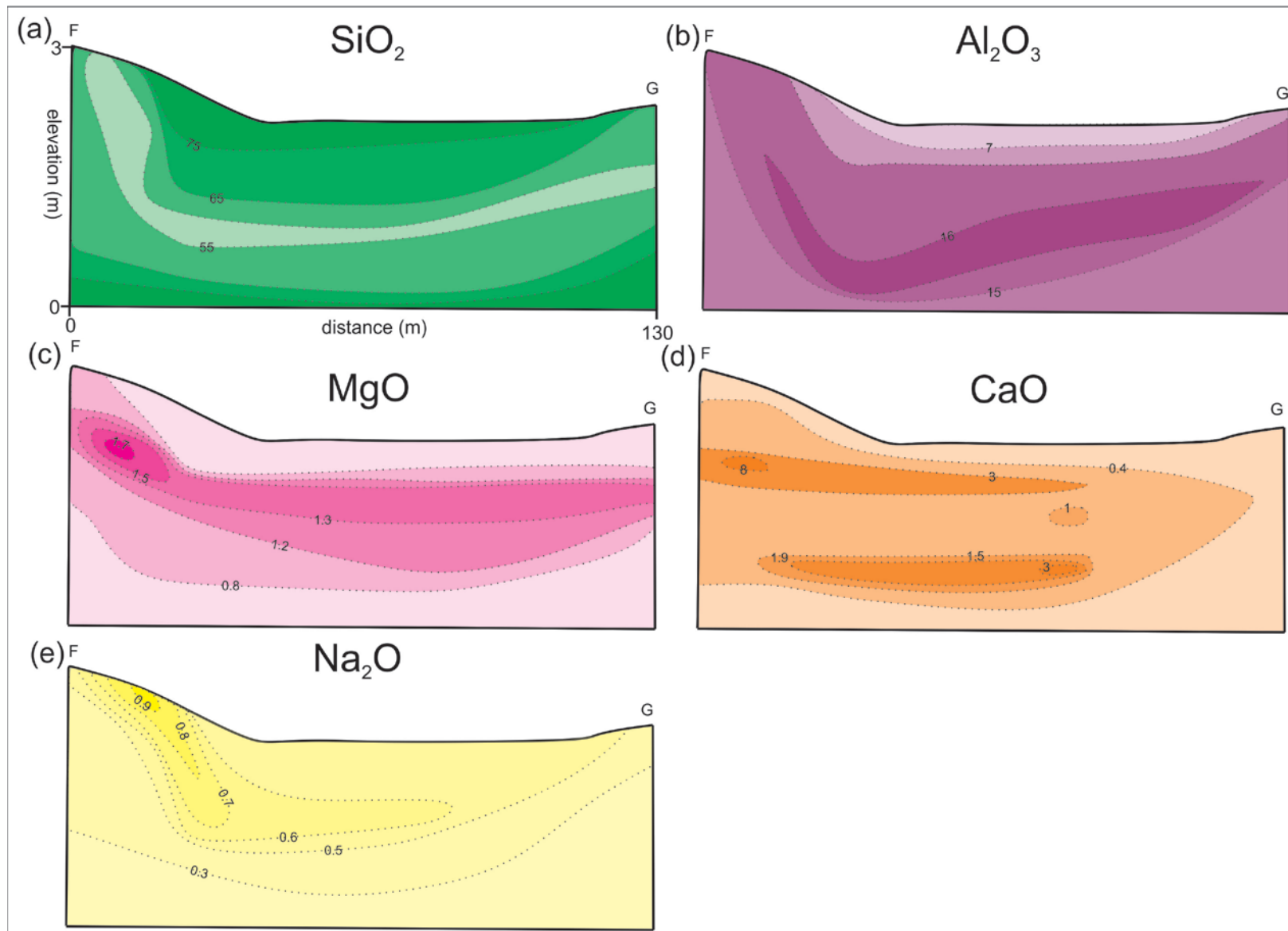
Figure 25: Subsurface geochemical isoline profiles across profile F-G

5.3   Mineralogy

The dominant mineral phase in the weathered materials was quartz, varying in abundance from 93 % to 19 %, with an average of 54.16 ± 20.37 (Table 10). Quartz was the only mineral phase present in all samples, being most abundant in the surface samples where the average concentration was 80.18 ± 5.77 wt %. Other common mineral phases were kaolinite, calcite, chlorite, dolomite and plagioclase (Table 10). Other minerals of interest that occur in the weathered materials are the iron-rich minerals magnetite, hematite, and goethite, and the titanium minerals rutile and anatase. On average, kaolinite was the second most abundant mineral, with an average of 25.91 ± 11.36; but it was not present in any surface samples.

Table 10: Mineralogy of samples in weight percent.

Sample	quartz	kaolinite	chlorite	calcite	dolomite	plagioclase	magnetite	geothite	hematite	muscovite	anatase	zircon	rutile
A1 0-10	80.46		9.32			7.85			2.37				
A1 70-75	43.00	22.90	12.82	15.29		3.10						2.94	
A1 100-110	35.62	30.89	7.23	3.23	23.04								
A1 150-160	40.80	32.96		13.83			1.40			11.05			
A2 0-10	93.22					6.78							
A2 60-70	24.48	53.00		5.80			1.79	5.47		9.49			
A2 120-130	28.30	17.00		25.36	29.33								
A2 180-190	35.00	28.50		5.76	23.43			7.23					
A3 0-10	79.20		4.87			9.63				6.31			
A3 60-70	29.74	39.60		23.00							5.29	2.35	
A3 80-90	16.67	9.59		67.56							1.74	4.44	
A3 130-140	19.57	20.67		38.71	21.06								
A4 0-10	77.00		10.10			4.88		7.95					
A4 60-70	71.43	6.27	10.42	8.07		3.81							
A4 120-130	53.25	14.71	19.60			12.44							
A4 160-170	46.36	27.20	16.96		9.48								
A5 0-10	76.38		9.69		0.00	13.93							
A5 50-60	54.10	24.20	21.70										
A5 120-130	62.32	31.66	6.02										
A5 150-160	44.30	38.90	16.80										
A5 185-190	55.60	31.80	10.98				1.53						
A5 210-220	88.73									4.85	6.42		
A6 0-10	76.22		8.20			15.57							
A6 60-70	54.20	16.90	16.41	3.80		6.53	2.13						
A6 80-90	34.07	13.85	10.16	31.49		7.24	3.19						
A6 140-145	53.91	27.80	7.28			3.72		6.51				0.77	
A7 0-10	82.68							6.69	8.47				2.15
A7 60-70	49.00	20.82	10.29							15.60	4.29		
A7 70-80	71.40		16.10					12.45					
AC 0-10	76.24		13.62			10.14							
AC 40-50	61.40	13.92	15.00			9.65							
AC 50-60	51.90	16.14	15.43	7.26		8.21	1.07						
AC 90-100	53.50	22.80	23.70										
AC 110-120	42.60	46.30	11.12										
AC 130-140	32.55	38.92	18.51	10.02									
AC 140-145	54.40	26.30	16.72	2.54									
Average	54.16	25.91	13.04	17.45	17.72	8.23	1.85	7.72	5.50	10.64	3.77	2.63	2.15
Std Dev	20.37	11.36	4.92	17.73	10.85	3.73	0.75	2.46	2.56	3.83	1.83	1.52	

Concentrations of the dominant minerals in and across cores are shown for transects C-E (Figure 26) and F-G (Figure 27). There was enrichment of calcite at mid-depths in cores A1-A3, but the abundance of calcite decreased markedly towards the centre of the pan for Transect C-E (Figure 26a). Across profile F-G, calcite did not occur in high concentrations, although it was present in a limited number of samples at very low concentrations.

Dolomite did not occur in cores A4-A7 in Transect F-G but it was present in cores A1-A3 in Transect C-E at intermediate depths (Figure 26b). Dolomite concentrations were greatest at mid-depths in cores A1-A3 and decreased towards the centre of the pan.

Plagioclase, was present in near-surface samples such that its concentration decreased with increasing depth in both profiles C-E (Figure 26c) and F-G (Figure 27a). There was no strong lateral variation in the distribution of plagioclase across the Transects.

Subsurface distribution of quartz showed an increase in concentration laterally towards the centre of the pan, with the lowest concentration in any given core being measured at intermediate depths in profile C-E (Figure 26d). Transect F-G showed the same overall trend but had a zone of relatively high quartz concentration at intermediate depths (Figure 27b).

Kaolinite concentration was greatest at intermediate depths for both profiles C-E (Figure 26e) and F-G (Figure 27c). In addition to these vertical trends in kaolinite variation, kaolinite concentrations largely increased laterally towards the centre of the pan.

Chlorite concentration was greatest at the centre of the pan, decreasing laterally from the centre of the pan to the surrounding areas. Chlorite concentration was greater in the samples A4-A6 of Transect F-G (Figure 27d) than in samples A1-A3 on Transect C-E (Figure 26f).
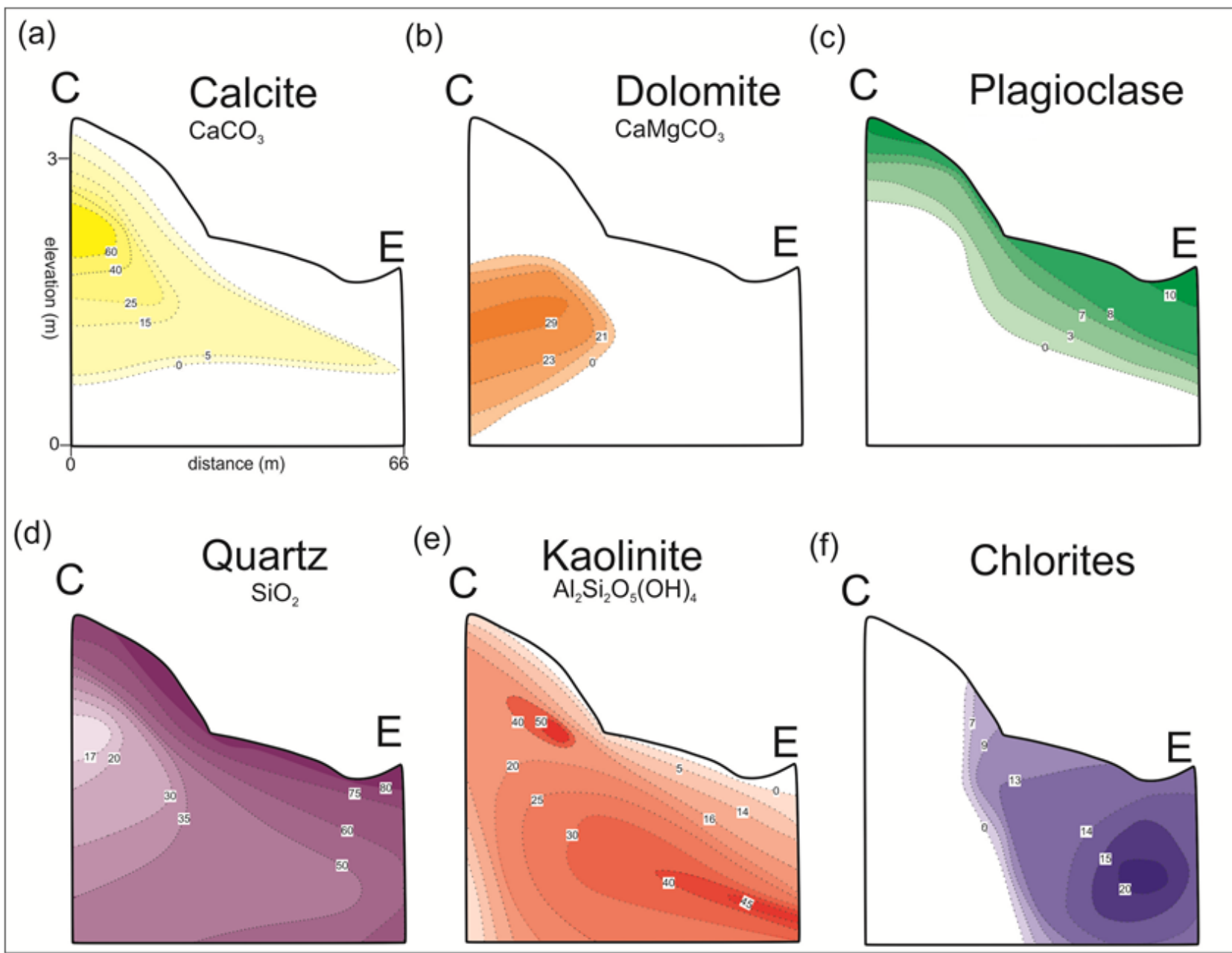
Figure 26: Subsurface isoline profile of mineralogy across profile C-E. Isolines are in percentages.
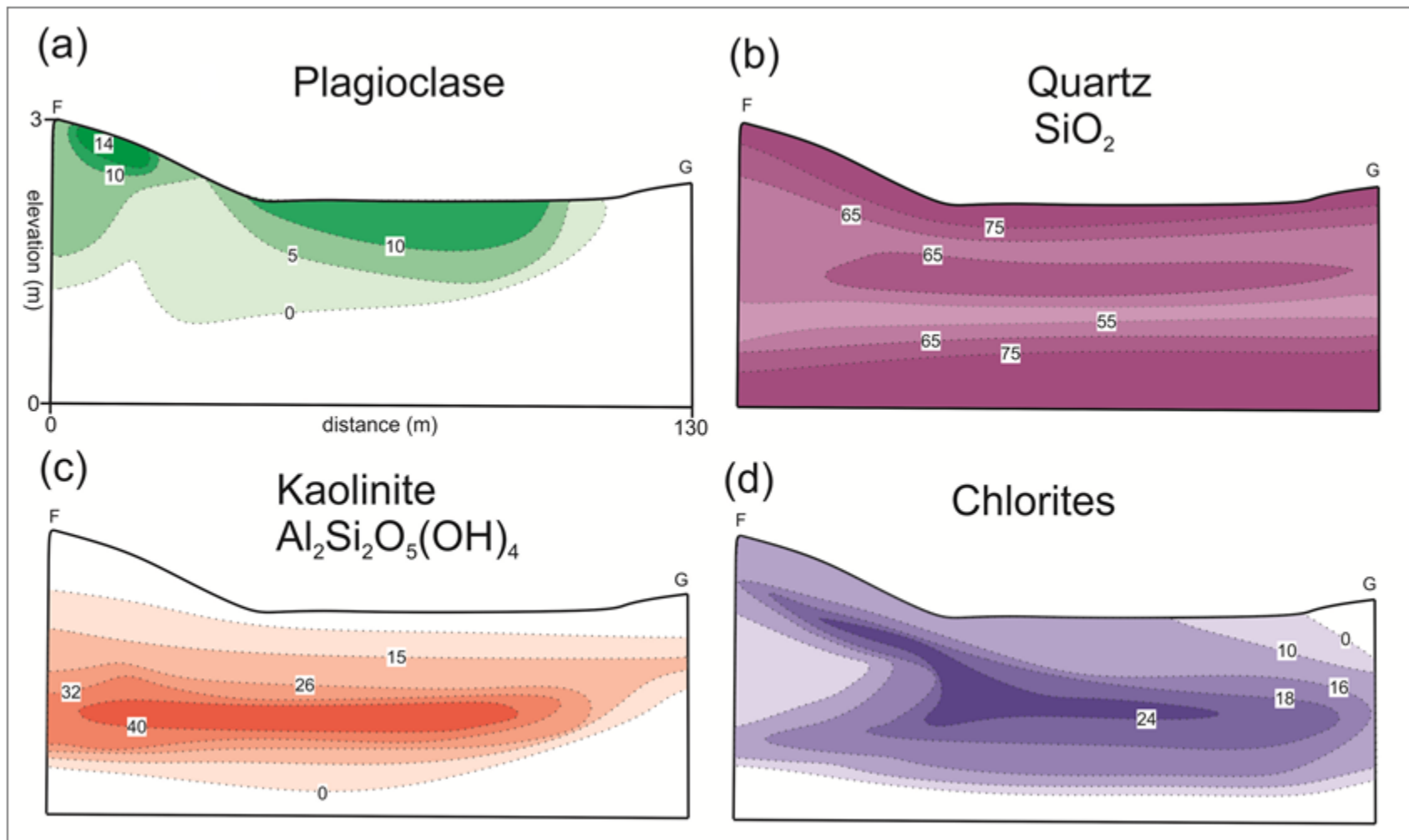
Figure 27: Subsurface isoline profile of mineralogy across profile F-G. Isolines are in percentages.

5.4   Parent Rock Geochemistry and Mineralogy

The tillite sample from a deep core nearby consisted predominantly of SiO_2 which made up 67.29 wt % of the composition. The only other notably high concentration was Al_2O_3 which occurred at a concentration of 14.29 wt %. CaO, MgO, K_2O, Na_2O and Fe_2O_3 were present between 2-5 wt % (Table 11).

Table 11: Major element geochemical composition of tillite (parent material) represented in terms of weight percent.

Weight %	Tillite
SiO_2	67.29
TiO_2	0.68
Al_2O_3	14.29
Fe_2O_3	5.48
MnO	0.09
MgO	2.09
CaO	2.12
Na_2O	3.09
K_2O	3.14
P_2O_5	0.17
Cr_2O_3	0.02
NiO	0.00
V_2O_5	0.02
ZrO_2	0.03
CuO	*<0.01*
LOI	2.54
TOTAL	101.05

The tillite samples consisted mainly of quartz and plagioclase, with lesser concentrations of microcline (K-feldspar), chlorite and muscovite (Table 12).

Table 12: Mineralogical composition of tillite (parent material) represented as weight percent.

Mineral	Chlorite	Microcline	Muscovite	Plagioclase	Quartz
Weight%	11.63	12.44	5.17	33.04	37.72

5.5   Degree of weathering

The results for the chemical weathering indices Chemical Index of Alteration (CIA), Parker's Weathering Index (WIP), and the Chemical Index of Weathering (CIW) have been plotted in Figure 28 such that scores change from left to right to reflect increasing weathering. Results for the CIA and WIP indicated that there was a negative relationship between depth and the degree of weathering such that samples at greatest depth were poorly weathered while shallow samples were highly weathered (Figure 28a and Figure 28b). Results for the same two indices showed that the core at the centre of the pan was highly weathered irrespective of depth.

The CIW results showed similar trends to those exhibited by WIP and CIA, but suggested much lower degrees of weathering (Figure 28c). For the CIW the highest degree of weathering occurred in surface samples. Samples at the centre of the pan showed modest degrees of weathering, while fringe deep subsurface samples indicated a slight degree of weathering.
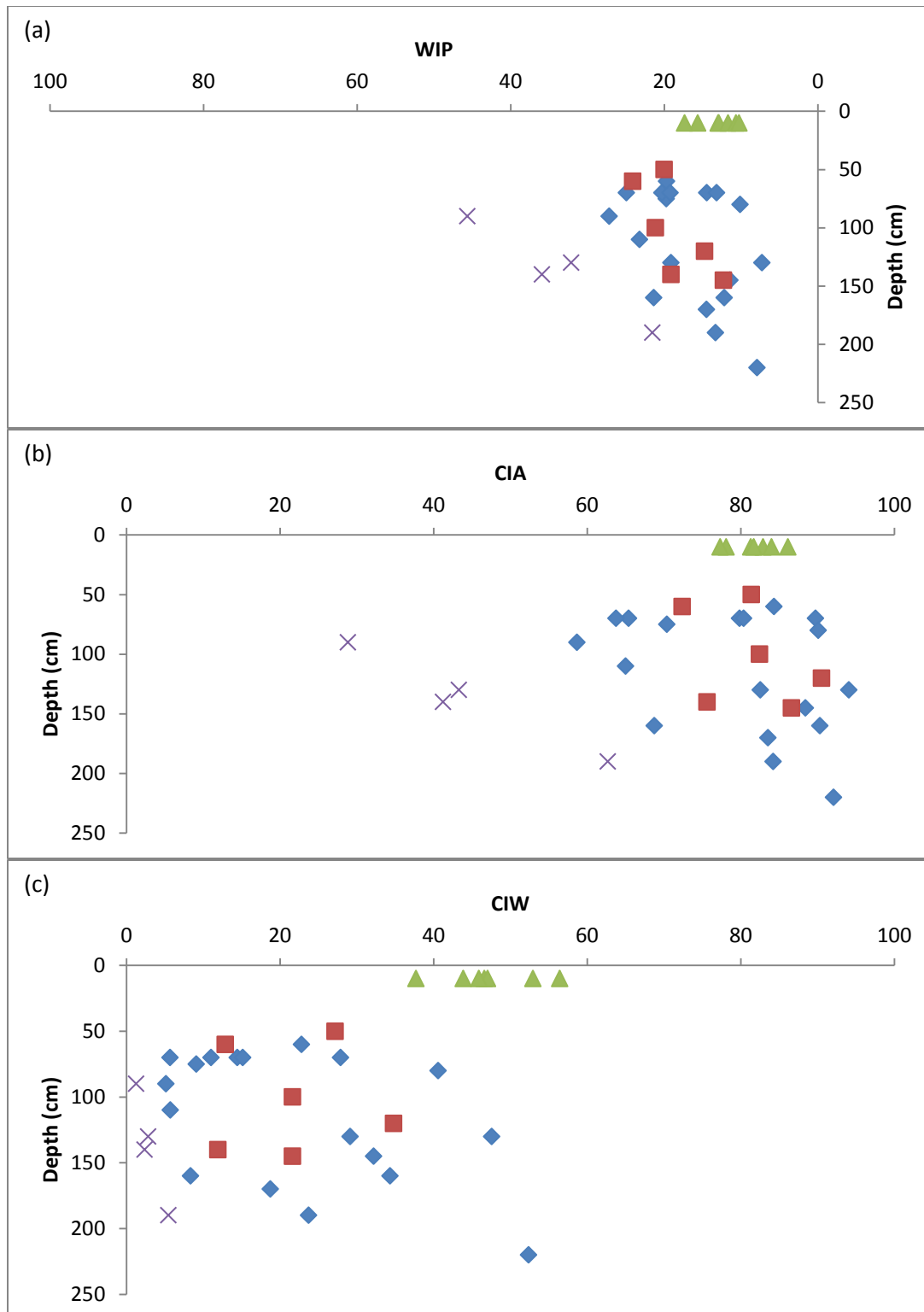
Figure 28: WIP (a), CIA (b) and CIW (c) index results plotted against depth of sampling. Blue diamonds represent subsurface samples and green triangles represent surface samples for cores on the fringe of the pan (A1 to A7), while red squares represent samples from the core in the centre of the pan (AC). Purple crosses represent a subset of samples taken at greatest depths in the highest-lying cores (A2 and A3).

5.6 Volume Changes

Volume change due to weathering within and between cores were variable (Figure 29). All samples taken at the soil surface (0 to 10 cm depth) showed considerable volume reductions. Core A4 was the only core that indicated a volume reduction at all depths. By excluding surface samples (which demonstrate relatively high degrees of volume loss) from the cores there was a positive relationship between volume loss and depth, with the strength of the relationship decreasing outwards toward the fringes of the pan (A1: $R^2 = 0.67$, A5: $R^2 = 0.37$, and A6: $R^2 = 0.11$). The core with the most seemingly variable volume change results was the centre core AC, not in terms of the degree of volume change but rather where there was no consistent observable trend between volume change and depth.
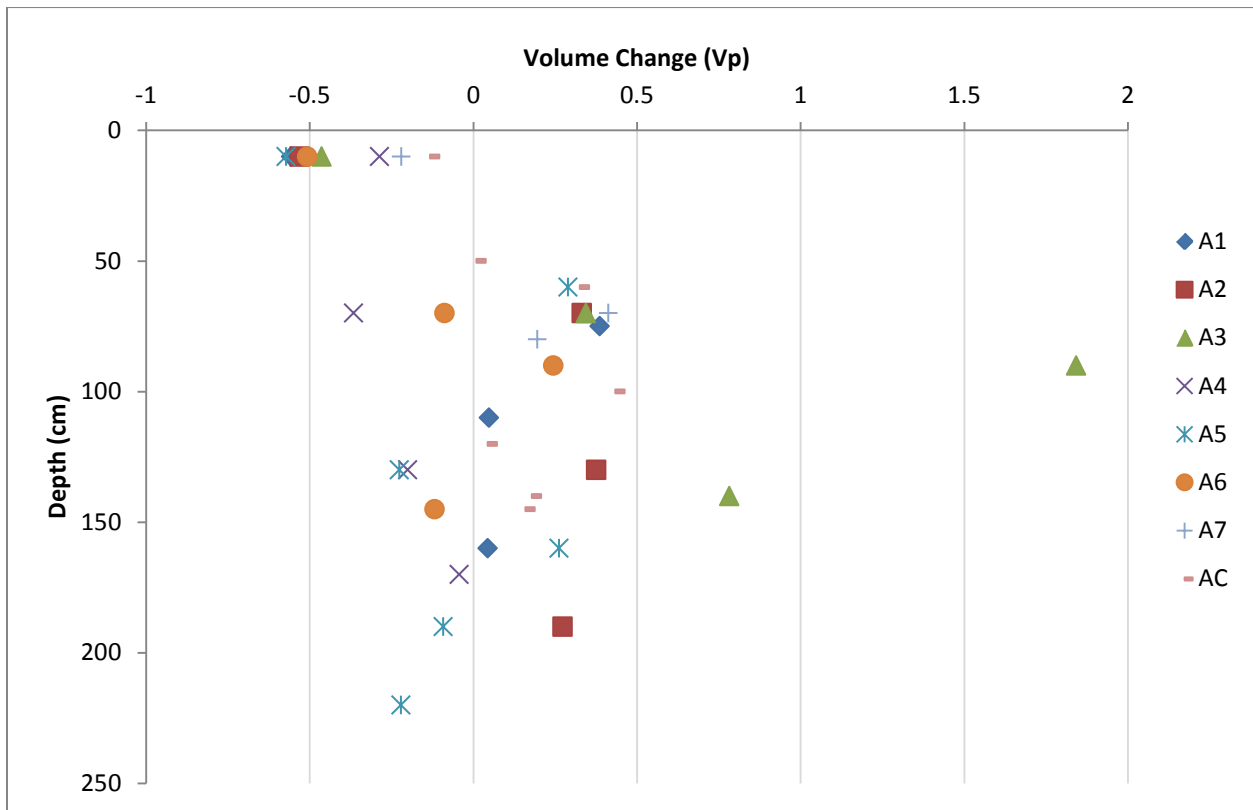
Figure 29: Volume change index results plotted against depth for samples in all cores. Values above zero indicate volume expansion and values below zero indicate volume reduction.

Chapter 6: Discussion

6.1 Introduction

Based on soil geochemical and mineralogical analyses there is a definite possibility for mass and volume changes to occur locally in the area of the current pan that are fairly consistent with the local topography. Based on calculations showing volume loss per core rather than per sample, mass loss occurs mainly in the pan itself while volume gains or small volume losses occur on the periphery of the pan (Figure 30).
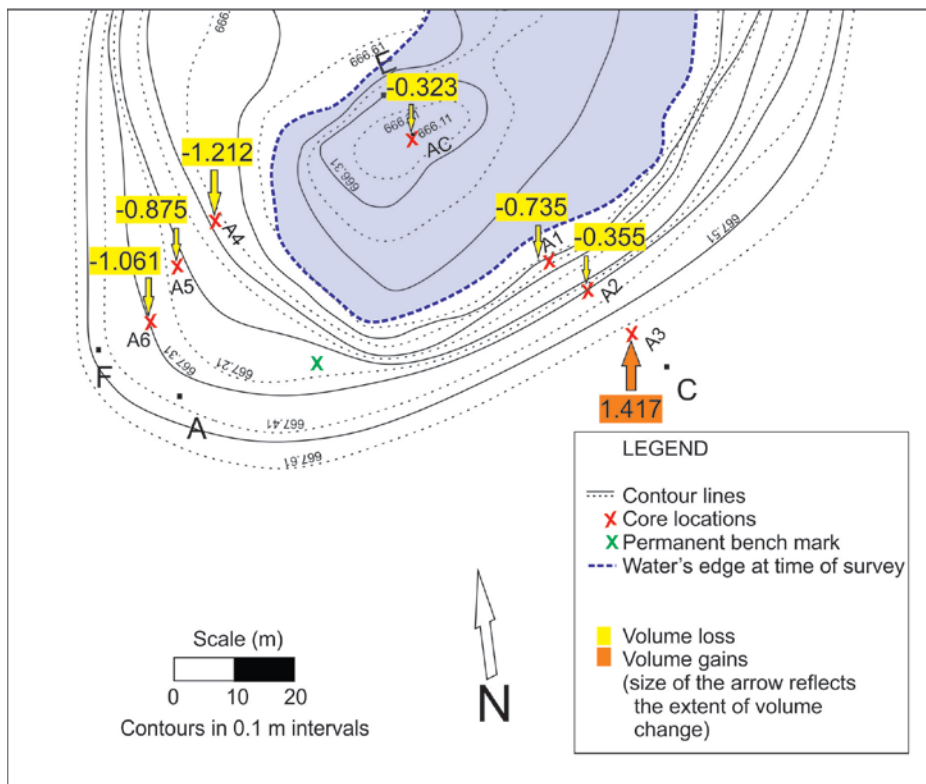
Figure 30: Volume change results per core, presented on a map of part of the pan.

There is a weak positive correlation, between relative elevation and volume changes such that areas at the highest relative elevations were associated with the highest volume gain, while areas at the lowest elevations were associated with the greatest volume loss (Figure 31). It is proposed that mass loss occurs largely due to deep weathering and mineralogical simplification (kaolinisation and silcrete formation), while the mass gain is likely to be a consequence of lateral

movement of solutes from the pan centre to the pan margin driven by transpirational water loss by emergent vegetation on the edge of the pan.
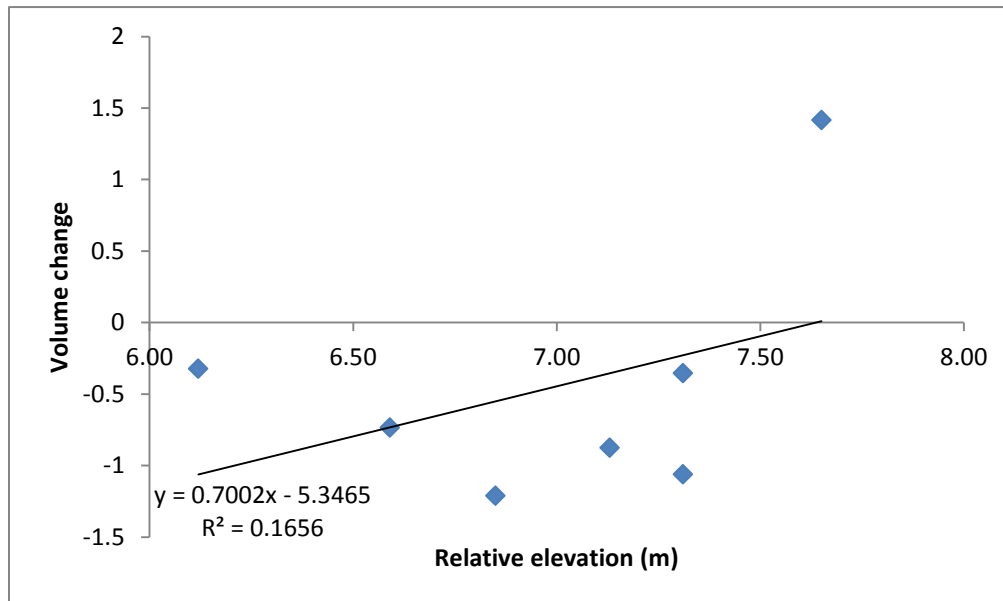
Figure 31: Relationship between the volume loss and elevation of the land surface of each core as calculated over a depth of 0 to 1.60 m.

It is evident in this study that the water surface in the pan was elevated relative to groundwater surface, and that groundwater recharge from the pan to the regional water table must therefore take place – albeit probably to a limited degree at present as the water level in the pan dropped very slowly during periods of no rainfall.

Aggradation due to chemical sedimentation associated with the lateral movement of water occurs on islands in the Okavango Delta in Botswana (Ellery *et al.,* 1993; McCarthy *et al.,* 1993; McCarthy and Ellery, 1994; McCarthy and Ellery, 1995; McCarthy *et al.,* 1998) and the Mkuze floodplain in KwaZulu-Natal (Humphries *et al.,* 2010a; Humphries *et al.,* 2010b; Humphries *et al.,* 2011a; Humphries *et al.,* 2011b). I will therefore argue that the origin of this pan – and possibly of pans generally on the African Erosion Surface near Grahamstown – are due to geochemical processes associated with deep weathering (acts to redistribute solutes vertically) and transpirational water loss in a groundwater recharge system (acts to redistribute solutes

laterally), leading to volume loss and volume gain respectively and the creation of a closed drainage basin.

Given the processes described above it is clear that pan evolution takes place over extended periods of time (probably tens of millions of years), as that is the time scale involved in the formation of pedogenic silcretes, whose presence in this study is a critical factor. The processes leading to pan formation and evolution do not necessarily act uniformly over the period of pan formation and evolution, and there must be factors initiating pan formation to start with. An attempt will thus be made to explain the processes leading to pan formation and evolution that will be summarised in a conceptual model.

The data in the study also allows for an interpretation of the weathering sequence of tillite over an extremely long time period, and an attempt will also be made to describe a possible weathering sequence.

6.2   Pan Origins

The pan is situated on the African Erosion Surface near Grahamstown on the King Flats, which is a remarkably flat surface with slopes generally less than 2 % and typically less than 1%. The pan is situated above the highest local contour of 660 m such that it receives runoff from a very localised catchment, which has a radius of approximately 240 m and an area of less than 20 ha. Given that it occurs in a region of low rainfall (less than 600mm/a) runoff does not move across the landscape in large quantities or at high velocities.

Given such a flat surface of this nature small local depressions up to a scale of about 10 m with local relief of centimetres to approximately 10 cm occur, which lead to limited ponding following rainfall. The origin of these depressions is unclear and needs further investigation, but these depressions are present on the land surface around the pan, only to be seen during rainfall events when small shallow pools are present and persist for days after the rainfall event. I speculate that localised depressions may arise through geological factors such as faults or small scale fractures in the bedrock, or even intrusions of rock that weathers differently to the regional parent material (Tooth *et al.,* 2000) or even biological factors such as animal activity, probably burrowing or mound-building animals that redistribute clastic material locally in the landscape at

a scale of tens of metres (McCarthy *et al.,* 1998; Dangerfield *et al.,* 1998; Ellery *et al.,* 1998). Understanding the origin of such local scale microrelief is beyond the scope of this study and will probably be difficult to determine. This leads to a range of scientific challenges, but a likely source of new insights here may be in the examination of pans on bedrock, such as those on the Highveld of South Africa as well as on quartzite along the southern Cape foothills of the Langeberg Mountains and its western extensions. However, once a shallow pond forms, hydration of underlying rock is favoured, promoting weathering at a greater rate than in adjacent elevated areas.

6.3   Deep weathering and volume loss

Given ponding in the landscape, local hydration of rock and associated localised weathering is inevitable. Silcrete (microcrystalline quartz) and kaolinite are the two important products of intense weathering both mineralogically and geochemically. Kaolinisation is greatest at mid depths, below this the degree of kaolinisation and content of silica increases. There is an important distinction from the findings that shows that where kaolinisation is greatest, silcrete content is lowest. Quartz content is highest near the surface. These findings indicate that the degree of weathering starts to decrease with depth following the decrease of kaolinite concentration and the increase of silica. It is clear that during this mineral simplification process, elements were redistributed. This redistribution of solutes influenced the lateral and vertical distribution of minerals which leads to a difference in rock density and hence the small scale volume changes. There is a relationship between the degree of weathering as determined by the WIP and volume changes (Figure 32), supporting the premise that the degree of weathering and the resultant mineral distribution is linked with the observed volume change.
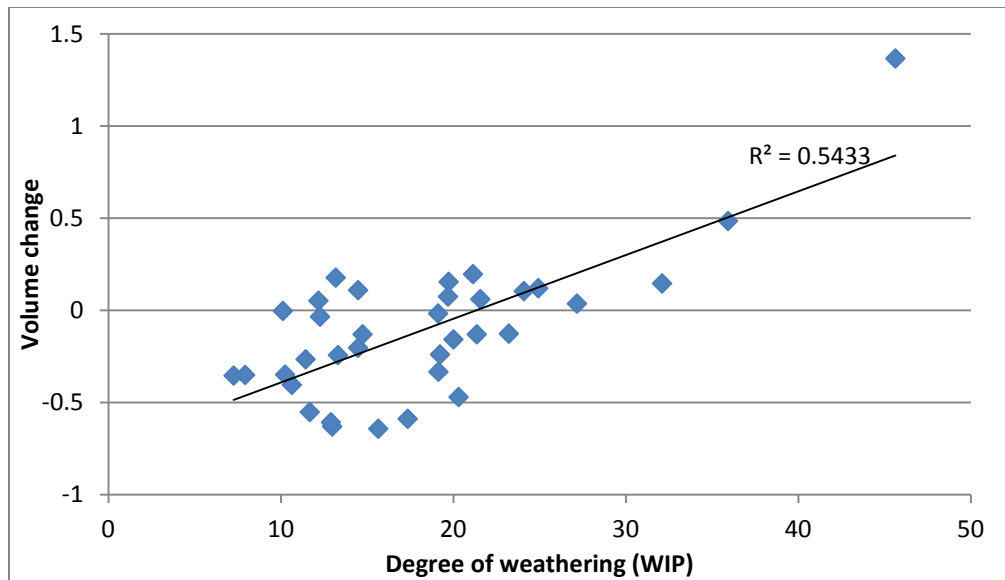
Figure 32: Relationship between the degree of weathering (WIP) and volume losses and gains (the degree of weathering is highest at zero on the WIP)

Volume gains show a strong negative relationship with increasing SiO_2 content (Figure 33). This is expected at surface conditions since the silcrete layers are highly differentiated and lack any other significant mineralogy, but the trend is consistent even when surface samples are excluded.
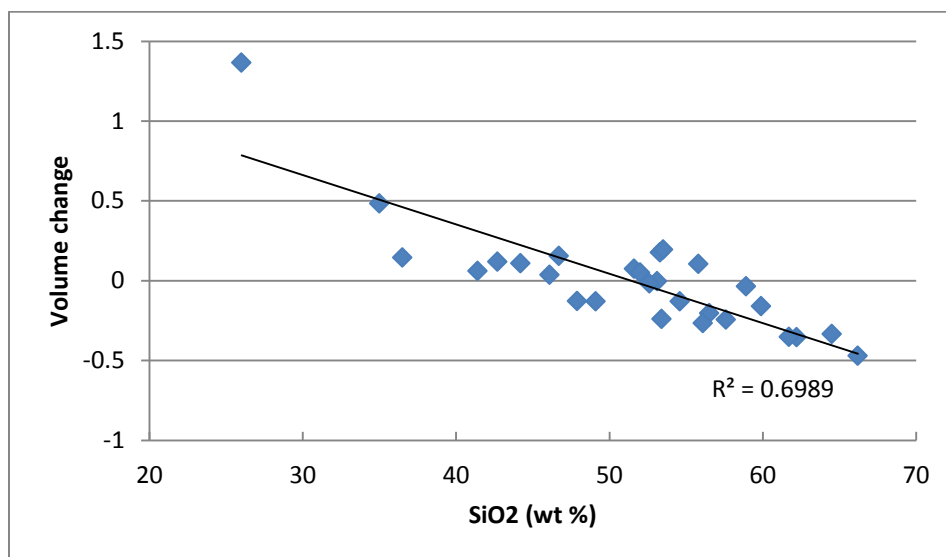
Figure 33: Relationship between SiO_2 content and volume losses and gains

6.4 Lateral movement of solutes and volume gain surrounding the pan

Once a depression forms and fills with water during the early phase of pan evolution, when bedrock is either at a very shallow depth or at surface, vegetation on the floor of the pan is unable to establish because of the lack of soils on the floor of the depression. In a semi-arid environment, runoff into the depression will likely elevate the water surface in the depression to a greater elevation than the water table in the surrounding landscape, leading to groundwater recharge from the depression. This leads to the net flux of water and solutes from the depression to the surrounding landscape, where transpirational water loss associated with selective uptake of solutes by plants on the fringes of the depression leads to precipitation of excluded solutes in the soil.

A group of scientists working in the Okavango Delta in Botswana have shown that evergreen trees that occur on the fringes of islands are rooted in the water table (Ellery *et al.,* 1993a, and Ellery *et al.,* 1993b). Because of their high leaf area index these trees transpire large quantities of water from the groundwater table (Ellery *et al.,* 1993a). This lowers the water table beneath the island relative to the surrounding swamp, such that groundwater recharge from the edge of the island to the centre of the island is ongoing (Figure 34). Due to the selective uptake of water and exclusion of solutes, groundwater is increasingly enriched in solutes to a point where calcium and magnesium carbonate precipitates from solution in the soil, creating topographic relief (Ellery *et al.,* 1993b). The co-incidence of high calcium and magnesium carbonate concentrations in the soil with areas of greatest woody vegetation cover and highest relief, supports this suggestion. Solute enrichment leads to an increase in electrical conductivity from the edge of the island to the centre, such that vegetation in the centre of the islands is eventually poisoned by toxic salts. This combination of processes leads to islands that have a rim of high-lying ground around the edge of the island that surrounds a central depression with saline soils.

Similar discoveries have been made in the Mkuze Wetland in KwaZulu-Natal, where transpiration by trees is considered to lead to floodplain aggradation, and where this occurs in groundwater recharge zones adjacent to the floodplain, aggradation of the floodplain margin is widespread (Humphries *et al.,* 2010a; Humphries *et al.,* 2010b; Humphries *et al.,* 2011a; Humphries *et al.,* 2011b).
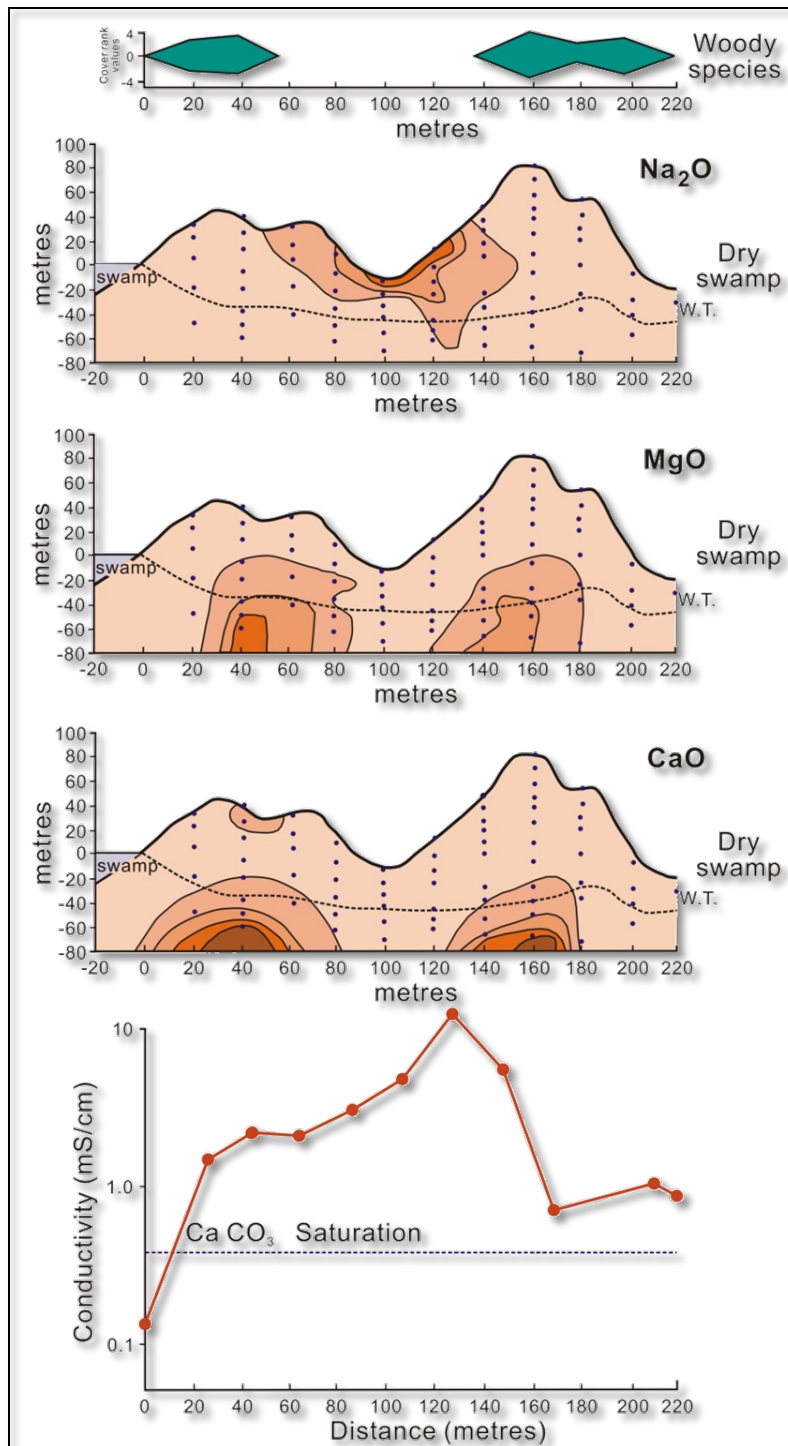
Figure 34: Effect of vegetation on carbonate saturation, and element distribution in the sub surface of island fringes in the Okavango Delta (Ellery *et al.,* 1993).

In the case of pans on the African Erosion Surface near Grahamstown, the processes are similar but groundwater recharge happens in the opposite direction – i.e. from a localised depression into the surrounding landscape. Data in this study suggests that solutes in the pan flowing into the surrounding landscape, in association with transpiration by fringing vegetation, may lead to the accumulation of calcium and magnesium carbonate in the soils around the pan, creating topographic relief. Indeed across the pan there is a positive relationship between volume changes and CaO and calcite concentrations (Figure 35a and 35b). These processes seem likely to dominate during early pan evolution, as the current water table is well below the zone of carbonate enrichment and therefore cannot be an important process at present.

Figure 35: Volume changes versus (a) CaO concentrations and (b) calcite concentrations.

6.5 Proposed model for pan formation on the African Erosion Surface near Grahamstown

A pre-existing small depression (Figure 36a) in a topographically flat area provides a starting point for pan development. This small depression gets filled with surface runoff from a loc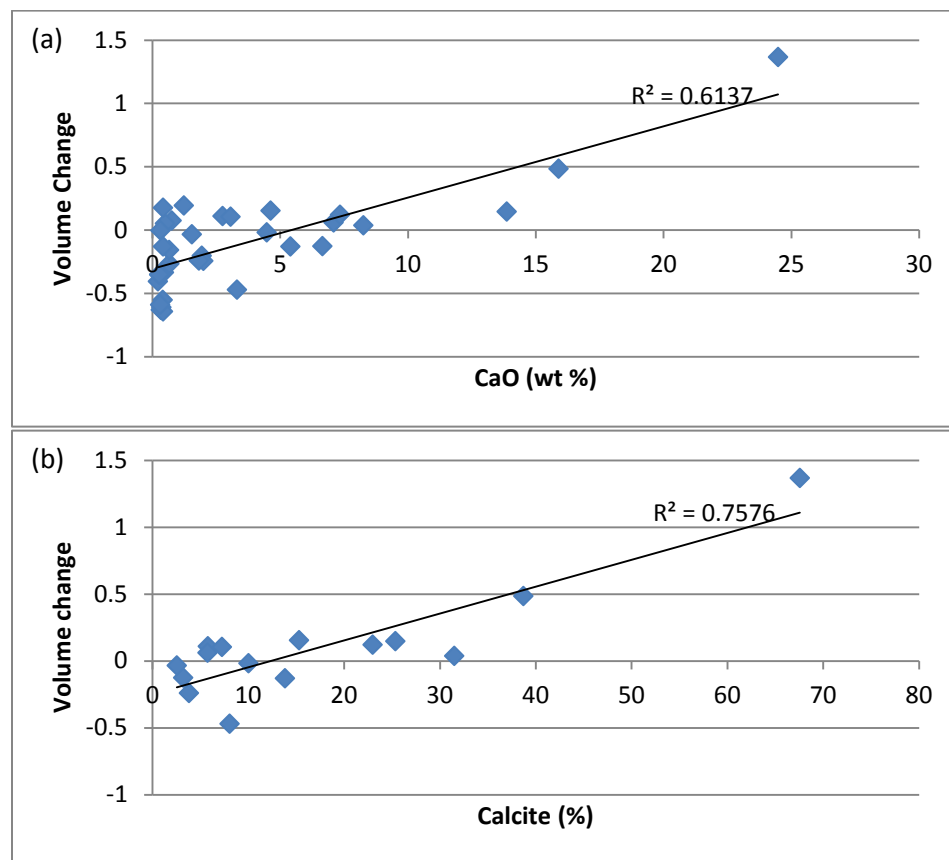al surrounding catchment, and recharges the local water table. Interaction of the rock with the infiltrating water increases the rate of weathering in a localized pocket (Figure 36b) relative to the degree of weathering occurring in the surrounding parent rock. The normal progression of weathering takes place, where hydrolysis breaks down mineral constituents into solution and redistributes them vertically and horizontally in the landscape. Si moves vertically, as is the norm during pedogenic silcrete formation at surface, while contemporaneously kaolinite forms at depth below the silcrete. During this process the vegetation which has established on the margins of the depression, causes the lateral movement of more readily mobile solutes such as Ca and Mg, away from the centre of the depression to be deposited laterally and create topographic relief (Figure 36c). This removal of solutes from the basin centre is greater than from the surrounding rock mass, as the availability of solutes is increased by the higher water availability from ponding in the depression. This causes a mass loss in the centre of depression and leads to volume reduction (Figure 36d), and consequent deepening of the basin. The selective exclusion of solutes such as Ca and Mg by the vegetation results in their sub surface accumulation adjacent to the depression (Figure 36c) forming Ca and Mg carbonates along the margins of the pan (Figure 36d). The precipitation of carbonates causes volume expansion, marginally increasing the elevation along the fringes of the pan. The current depth of the water table beneath the pan suggests that the water table must have lowered gradually over time (Figure 36d), due probably to altered hydraulic properties of the pan fringe as a consequence of solute precipitation.
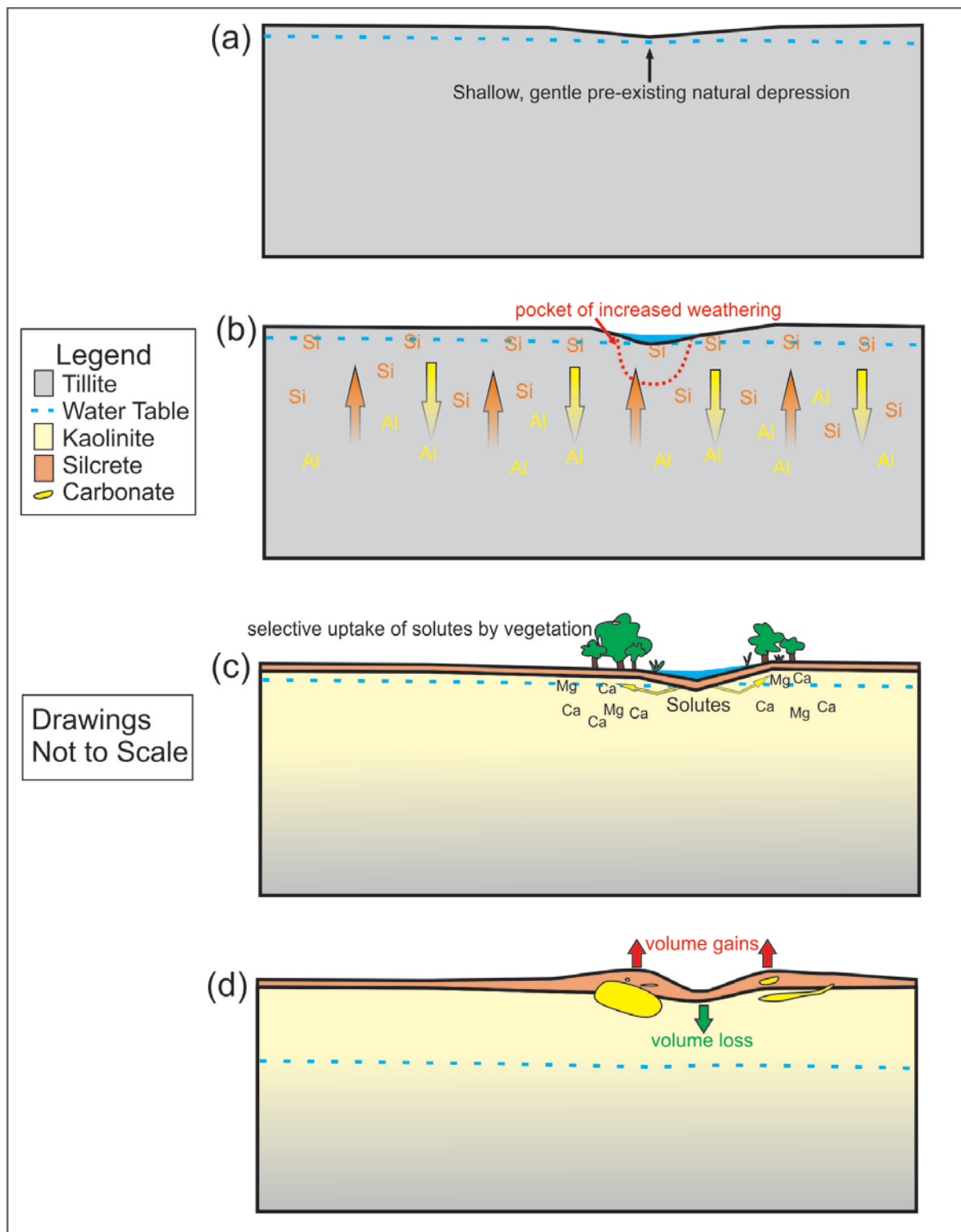
Figure 36: Conceptual model for pan formation in the African Erosion Surface near Grahamstown.

6.6　Further Research

Future research on this topic should increase our understanding of a number of issues realized in this study, the first of which is the need to more accurately link elevation with local scale volume changes in various weathering settings in South Africa, and perhaps in other settings where fringe vegetation dominates and hence lateral migration of solutes occurs.

The origin of micorelief features, such as those that are proposed to have initiated pan propagation in this study, is unknown. Additionally the significance of such microrelief depressions in terms of geological age could help to understand better the timescale over which pan propagation on the African Erosion Surface occurs. In this regard, suggestions for potential insights from pans in the Highveld of South Africa as well as on quartzite plains along the southern Cape foothills of the Langeberg Mountains, have already been made.

Chapter 7: Conclusions

The dominant processes surrounding pans, and indeed wetlands in general, centre around the role of hydrological and biological processes. This study by no means intends to undermine the importance of such sciences, but rather attempts to shed light on processes belonging to geomorphological and geological sciences. The clear distinction in timescales over which biological and geological processes occur should affect the manner in which wetlands are viewed. Because of the dominance of the biological and hydrological discourses, wetlands and wetland problems are often viewed in terms of fast variables of change, which although in many cases is sufficiently accurate for wise management, there are times when appreciation of slow variables of change may be more useful, especially when attempting to understand the natural evolution of a system. This study shows that process occurring over millions of years may be responsible for the formation of pans on the African Erosion Surface near Grahamstown, and that indeed the models relying on recent dynamics such as overgrazing and deflation, are unlikely to have caused pan propagation in this particular environmental setting on the African Erosion Surface. These results provide a foundation for future research on local scale volume changes and their effect on shaping the landscape.

Results show that due to prolonged chemical weathering, which has been intensified by ponding of water in a small depression, volume changes may occur that are associated with measurable changes in relief within and around the margins of a depression. Mineralogical and geochemical results have linked increasing Si concentrations with volume losses, and increasing Ca and Mg concentrations as magnesian calcite with volume gains.

The insights gained in this study concerning pan origin and evolution on the African Erosion Surface highlight the ancient (geological) origin of these natural features. Conventional conservation planning has a strictly ecological focus around biodiversity and ecosystem preservation. Given the length of time taken to form these depression wetlands around Grahamstown and possibly elsewhere, and the fact that once destroyed these remarkable features will not form again naturally over many millions of years, I would like to propose that the degradation and destruction of pans should be halted, and that further research should be undertaken to strengthen our understanding of slow-forming features as these are an important

part of our natural heritage. Furthermore, the pans around Grahamstown are host to a limited number of endemic taxa, including the vlei lily *Crinum campanulatum*, which produces a spectacular show during wet seasons and is a flagship for these remarkable depression features that characterise the Eastern Cape between East London and Nanaga, east of Port Elizabeth.

Figure 37: The vlei lily *Crinum campanulatum* (photograph taken by Fred Ellery)

References

Allan DG, Seaman MT, Kaletja B. (1995). The endorheic pans of South Africa. In: Cowan, GI. (Eds), Wetlands of South Africa. Department of Environmental Affairs and Tourism, Pretoria, South Africa. 75-101.

Bahlburg H and Dobrzinski N. (2011). A review of the Chemical Index of Alteration (CIA) and its application to study of Neoproterozoic glacial deposits and climate transitions. *Geological Society, London, Memoirs* 36, 81-92.

Birkeland PW. (1984). Soils and Geomorphology. Oxford Univ. Press, 372.

Blodau, C. (2006). A review of acidity generation and consumption in acidic coal mine lakes and their watersheds, *Science of the Total Environment*, 369 (1–3), 307–332

Bordy EM, Hancox PJ, Rubidge BS. (2004). Basin development during the deposition of the Elliot Formation (Late Triassic - Early Jurassic), Karoo Supergroup, South Africa. *South African Journal of Geology*, 10 (3), 397-412.

Carroll D. (1970). Rock Weathering. Plenum Press. New York.

Catuneanu O, Guiraud R, Eriksson PG, Thomas R, Shone R, and Key R. (eds.), (2005). Phanerozoic Evolution of Africa. *Journal of African Earth Sciences*, 43/1-3, 410

Catuneanu O, Hancox PJ, and Rubidge BS. (1998). Reciprocal flexural behaviour and contrasting stratigraphies: a new basin development model for the Karoo retroarc foreland system, South Africa. *Basin Research*, 10, 417-439.

Cooke RU and Warren A. (1973). Geomorphology in Deserts. Tiptree, London, England.

Dangerfield JM, McCarthy TS & Ellery WN. (1998). The mound building termite *Macrotermes michaelseni* as an ecosystem engineer. *Journal of Tropical Ecology,* 14, 507-520.

Davenport NA and Gambiza J. (2009). Municipal commonage policy and livestock owners: Findings from the Eastern Cape, South Africa. *Land Use Policy,* 26, 513-520.

Davenport NA, Shackleton CM and Gambiza J. (2012). The direct use value of municipal commonage goods and services to urban households in the Eastern Cape, South Africa, *Land Use Policy,* 29, 548-557.

Dini J, Cowan GI, and Goodman P. (1998). South African National Wetland Inventory. Proposed wetland classification system for South Africa. Department of Environmental Affairs and Tourism, Pretoria, South Africa.

Duzgoren-Aydin NS, Aydin A, Malpas J. (2002). Re-assessment of chemical weathering indices: case study on pyroclastic rocks of Hong Kong, *Engineering Geology,* 63, 99-119.

Edwards R. (2009) The origin and evolution of Dartmoor Vlei in the Kwazulu-Natal Midlands, South Africa. MSc. University of KwaZulu-Natal.

Ellery WN, Grenfell MC, Grenfell SE, Kotze DC, McCarthy TS, Tooth S, Grundling P-L, Beckedahl H, le Maitre D and Ramsay L. (2009). WET-Origins: Controls on the distribution and dynamics of wetlands in South Africa. Water Research Commission, Pretoria. WRC Report No. TT 334/08.

Ellery WN, Ellery K and McCarthy TS. (1993) Plant distribution on islands of the Okavango Delta: Determinants and feedback interactions. *African Journal of Ecology,* 31,118-134.

Ellery WN, McCarthy TS & Dangerfield JM. (1998). Biotic factors in Mima mound development: Evidence from the floodplains of the Okavango Delta, Botswana. International *Journal of Ecology and Environmental Science,* 24, 293-313.

Goudie AS and Thomas DSG. (1985). Pans in southern Africa with particular reference to South Africa and Zimbabwe, *Z Geomorphol.,* 29, 1-19.

Goudie AS and Wells GL. (1995). The nature, distribution and formation of pans in arid zones, *Earth Science Reviews,* 38, 1-69.

Grenfell SE, Ellery WN and Grenfell MC. (2009). Geomorphology and dynamics of the Mfolozi River floodplain, KwaZulu-Natal, South Africa. *Geomorphology*, 107, 226–240.

Harnois L. (1988). The CIW index: A new chemical index of weathering, *Sedimentary Geology,* 55, 319-322.

Huber H, Koeberl C, McDonald I and Reimold WU. (2001). Geochemistry and petrology of Witwatersrand and Dwyka diamictites from South Africa: Search for an extraterrestrial component. *Geochimica et Cosmochimica Acta,* 65 (12), 2007-2016.

Humphries MS, Kindness A, Ellery WN and Hughes J. (2010). Sediment geochemistry, mineral precipitation and clay neoformation on the Mkuze River Floodplain, South Africa. *Geoderma,* 157, 15-26.

Humphries MS, Kindness A, Ellery WN, Hughes J and Benitez-Nelson CR. (2010). [137]Cs and ^{210}Pb derived sediment accumulation rates and their role in the long-term development of the Mkuze River floodplain, South Africa. *Geomorphology,* 119, 88-96.

Humphries MS, Kindness A, Ellery WN, Hughes J, Bond JK and Barnes KB. (2011). Vegetation influences on groundwater salinity and chemical heterogeneity in a freshwater, recharge floodplain wetland, South Africa. *Journal of Hydrology,* 411, 130-139.

Humphries MS, Kindness A, Ellery WN and Hughes J. (2011). Water chemistry and effect of evapotranspiration on chemical sedimentation on the Mkuze River floodplain, South Africa. *Journal of Arid Environments,* 75, 555-565.

Hutchison CS. (1974). Laboratory Handbook of Petrographic Techniques. Wiley-Interscience, Toronto.

Jacob RE, Mitha VR, MacPherson D. (2004). The kaolinitic clay deposits on Beaconsfield, north of Grahamstown, *South African Journal of Science,* 100, 560-564.

Johnson MR, van Vuuren CJ, Visser JNJ, Cole DI, Wickens H de V, Christie ADM, Roberts DL, (1997) The Foreland Karoo Basin, South Africa. In: RC. Selly (eds): African Basins. Sedimentary Basins of the World, 3. Armsterdam: Elsevier Science B.V, 269-317.

Johnson MR, van Vuuren CJ, Visser JNJ, Cole DI, Wickens H de V, Christie ADM, Roberts DL, and Brandl G. (2006). Sedimentary rocks of the Karoo Supergroup. In: Johnson MR, Anhaeusser CR and Thomas RJ, (Eds.). The Geology of South Africa. Geological Society of South Africa, Johannesburg/ Council for Geoscience, Pretoria. pp. 461-499 Karoo Basin: Current Knowledge and Future Research Needs Prepared for the Water Research Commission. (Edited by Chevallier L.), WRC Report No. TT 179/02

Krzic M, Wiseman K, Dampier L, and Gaumont-Guay D. (2004). SoilWeb200: an on-line teaching tool for APBI 200 course. The University of British Columbia, Vancouver [online] Available: http://www.landfood.ubc.ca/soil200/index.htm

Le Roux JS. (1978). The Origin and distribution of pans in the Orange Free State. *South African Geography,* 6, 167-176.

Li C and Yang S. (2010). Is chemical index of alteration (CIA) a reliable proxy for chemical weathering in global drainage basins, *American Journal of Science,* 310, 111-127.

Marshell T, and Harmse JT, (1992). A review of the origin and propagation of pans, *South African Geographer,* 19, 9-21.

Maud RR. (1996). The Macro-Geomorphology of the Eastern Cape. IN: Lewis CA (Eds), The Geomorphology of the Eastern Cape, South Africa, Grocott and Sherry Publishers, Grahamstown, South Africa, 1-18.

McCarthy T, Cairncross B, Huizenga JM and Batchelor A. (2007). Conservation of the Mpumalanga Lakes District. [Online], Available: http://wetlands.sanbi.org/wfwet/articles2/Mpumalanga%20Lake%20District.pdf. (23/11/2012).

McCarthy TS, Ellery WN and Ellery K. (1993). Vegetation induced, subsurface precipitation of carbonate as an aggradational process in the permanent swamps of the Okavango (Delta) fan, Botswana. *Chemical Geology* 107, 111-131.

McCarthy, TS and Ellery WN. (1994). The effect of vegetation on soil and ground water chemistry and hydrology of islands in the seasonal swamps of the Okavango Fan, Botswana. *Journal of Hydrology* 154,169-193.

McCarthy, TS and Ellery WN. (1995). Sedimentation on the distal reaches of the Okavango Fan, Botswana, and its bearing on calcrete and silcrete (ganister) formation. *Journal of Sedimentary Research*, A65, 77-90.

McCarthy TS, Ellery WN and Dangerfield JM. (1998). The role of biota in the initiation and growth of islands on the floodplain of the Okavango Alluvial Fan, Botswana. *Earth Surface Processes and Landforms,* 23, 291-316.

McCarthy TS and Hancox PJ. (2000). Wetlands. IN: Partridge TC and Maud RR (Eds.), The Cenozoic of southern Africa: Oxford Monographs on Geology and Geophysics. Oxford University Press, Oxford, 218-235.

McCarthy TS and Rubidge B. (2005). The Story of Earth and Life: A southern African perspective on a 4.6-billion-year journey . Struik Publishers, Cape Town.

Nahon DB. (1991). Introduction to the petrology of soil and chemical weathering. John Wiley and Sons, USA.

Nash DJ and Ullyott JS, (2007). Silcretes. IN: Nash DJ and McLaren SJ (Eds), Geochemical Sediments and Landscapes. Blackwell Publishing, USA, 95-143.

National Water Act, 36 of 1998.

Nesbitt HW and Young GM. (1982). Early proterozoic climates and plate motions inferred from major element chemistry of lutites. *Nature,* 279, 715-717.

Norrish K and Hutton JT. (1969). An accurate X-ray spectrographic method for the analysis of a wide range of geological samples. *Geochimica et Cosmochimica Acta,* 33 (43), l-453.

Olsson MT and Melkerud P. (2000). Weathering in three podzolized pedons on glacial deposits in northern Sweden and central Finland, *Geoderma,* 94, 149-161.

Parker A. (1970). An index of weathering for silicate rocks. *Geol. Mag.,* 10, 501-504.

Price JR and Velbel MA. (2003). Chemical weathering indices applied to weathering profiles developed on heterogeneous felsic metamorphic parent rocks, *Chemical Geology,* 202, 397-416.

Polynov BB. (1937). The cycle of weathering; Translated by Muir A. Thomas Murby & Co. London.

Pote J, Shackleton C, Cocks M and Lubke R. (2006). Fuelwood harvesting and selection in Valley Thicket, South Africa, *Journal of Arid Environments,* 67, 270-287.

Rogers KH. (1997). Freshwater Wetlands. In: Cowling RM, Richardson DM and Pierce SM (Eds.), Vegetation of southern Africa. Cambridge University Press, 322-347.

Rosen MR. (1994) The importance of groundwater in playas. In: Rosen MR (Eds), Paleoclimate and Basin Evolution of Playa Systems. The Geological Society of America, Colorado, 1-18.

Schlesinger WH, (1996). In: Biogeochemistry — an Analysis of Global Change. Academic Press, 588.

Shackleton C, Gambiza J and Jones R. (2007). Household fuelwood use in small electrified towns of the Makana District, Eastern Cape, South Africa. *Journal of Energy in southern Africa*, 18 (3), 4-10.

Shao J, Yang S, Li C. (2012). Chemical indices (CIA and WIP) as proxies for integrated chemical weathering in China: Inferences from analysis of fluvial sediments, *Sedimentary Geology,* 265-266, 110-120.

Shaw PA. (1988). Lakes and Pans. In: Moon BP and Dardis GF (Eds.), The geomorphology of southern Africa: Southern Book Publishers, Johannesburg, 120-140.

Shaw PA and Thomas DSG. (1997). Pans, Playas, and Salt lakes. In: Thomas DSG (Eds), Arid Zone Geomorphology, Process, Form and Change in Drylands, 2nd Edition, John Willey and Sons, West Sussex, England, 293-319.

Smith RHM, Eriksson PG, and Botha WJ, (1993). A review of the stratigraphy and sedimentary environments of the Karoo-aged basins of southern Africa. Journal of African Earth Sciences, 16, 143-169.

Steynor A. (2006) Introduction to South African Climate. [Online], Available: http://www.climate.org.za/module_1. (23/11/2012).

Summerfield MA, (1984). Isovolumetric weathering and silcrete formation, southern Cape Province, South Africa, *Earth Surface Processes and Landforms,* 9, 135-141.

Summerfield MA, (1983). Silcrete as a palaeoclimate indicator: evidence from southern Africa, *Palaeogeography, Palaeoclimatology, Palaeoecology,* 41, 65-71.

Thomas DSG and Shaw PA. (1991). The Kalahari environment. Cambridge Univ. Press, 284.

Tooth S and McCarthy TS. (2007). Wetlands in drylands: geomorphological and sedimentological characteristics, with emphasis on examples from southern Africa. Progress in Physical Geography 31, 3-41.

Tooth S, McCarthy TS, Brandt D, Hancox PJ and Morris R. (2002). Geological controls on the formation of alluvial meanders and floodplain wetlands: The example of the Klip River, Eastern Free State, South Africa. *Earth Surface Processes and Landforms,* 27, 797-815.

Vogel C. (2000). Climate and climatic change: causes and consequences, In: Fox R and Rowntree K (eds), The Geography of South Africa in a changing world. Oxford University Press southern Africa, Cape Town, 284-302.

Webmineral (2012) Mineralogical Database, [Online] Available: www.webmineral.com

White AF, Blum AE, Shulz MS, Bullen TD, Harden JW and Peterson ML. (1996) Chemical weathering rates of a soil chronosequence on granitic alluvium: I. Quantification of mineralogical and surface area changes and calculation of primary silicate reaction rates. *Geochimica et Cosmochimica Acta,* 60 (14), 2533-2550.

Yatsu E. (1988). The nature of weathering: An Introduction. SOZOSHA. Japan.